1982

Relationship Between Soil Moisture and Soil Surface Temperature

Steven Darwin Ness

RELATIONSHIP BETWEEN SOIL MOISTURE
AND SOIL SURFACE TEMPERATURE

BY

STEVEN DARWIN NESS

A thesis submitted
in partial fulfillment of the requirements for the
degree of Master of Science
Major in Engineering
South Dakota State University
1982

RELATIONSHIP BETWEEN SOIL MOISTURE
AND SOIL SURFACE TEMPERATURE

This thesis is approved as a creditable and independent investigation by a candidate for the degree, Master of Science, and is acceptable as meeting the thesis requirements for this degree, but without implying that the conclusions reached by the candidate are necessarily the conclusions of the major department.

Dr. Jerald A. Tunheim   Date
Thesis Advisor

Dr. Jerald A. Tunheim   / Date
Head, Physics Department

ACKNOWLEDGEMENTS

TABLE OF CONTENTS

LIST OF FIGURES

LIST OF FIGURES (Contd)

LIST OF FIGURES (Contd)

LIST OF TABLES

INTRODUCTION

Thermal-infrared imagery (thermography) obtained from satellite altitudes has been shown to be a promising new tool for resource management and development. Satellite-borne thermal-infrared sensors allow the collection of time-sequential thermal-infrared radiation (thermal emittance) data over large land-surface areas of the earth at relatively low cost. Thus, any resource which can be related to thermal emittance can be readily monitored.

Thermal emittance from a surface is proportional to the fourth power of the surface temperature. Thus any factor which affects the surface temperature greatly affects the surface thermal emittance. Moisture is such a factor when the land surface is considered. Near-surface soil moisture changes the heat capacity and thermal conductivity of the soil and thus greatly alters the temperature of the land surface. Thermography is very sensitive to such changes in surface temperature making it a potentially useful tool for monitoring near-surface soil moisture.

Factors other than soil moisture also affect soil surface temperature and thus thermal emittance. These factors such as near-surface ground water, wind velocity, topography of the land, plant canopy, soil type, and other variables serve to complicate the method. Thus, the isolation of one factor such as soil moisture and its effect on thermal emittance is difficult. Therefore the interrelationship between these factors must be understood before a model that describes variations in thermal emittance can be constructed. The resource

scientist may then be able either to compensate for the effect of these factors during data analysis, or collect data when these factors have a minimal effect on the thermal emittance of the land-surface.

The plant canopy is a particular variable which must be understood and isolated since bare soil conditions of the land-surface are rare and usually temporary. Plant cover effectively shields the soil surface from solar radiation during the daylight hours reducing the total amount of energy supplied to the soil surface. It also insulates the soil from the atmosphere during the nighttime hours reducing the amount of heat escaping from the soil surface. These effects alter the thermal emittance of both the soil and plant canopy which together form the composite thermal image of the earth's surface as monitored by satellite.

The intervening atmosphere poses another particular problem when using satellite-borne sensors. It absorbs and emits components of thermal-infrared radiation thus affecting the amount actually reaching the satellite sensors. The temperature derived by assuming all radiation emitted from the earth reaches the satellite sensors may then differ greatly from the actual temperature of the earth's surface. The term "apparent temperature" is used to describe this remotely sensed variable.

The emissivity of the surface is dependent upon surface conditions. Since emissivity influences both the radiation absorbed and reflected by a surface, the apparent temperature will also depend on surface conditions.

Temperature differences between two points on the earth are easier to derive with reasonable accuracy from satellite thermal-infrared imagery (TIR) than the exact temperature of each point. If the atmospheric absorption and emission over both points is assumed identical and the emissivity is the same for both points, the apparent temperature difference will correspond very closely to the actual temperature difference for the two surfaces. For example, absorbtion by the atmosphere may decrease the satellite derived apparent temperatures of both points but the difference between these temperatures will be very close to the actual surface temperature difference.

A model that successfully relates apparent temperature differences between two points on the earth to soil moisture differences at the two points would allow the monitoring of soil moisture over large land-surface areas. This method would require the "ground truth" monitoring of soil moisture at a reference site. Satellite thermography would then be used to determine apparent temperature differences between the reference site and any number of other sites. Moisture differences between the reference site and other sites could then be calculated from the apparent temperature differences using the model. The general objective of this research was to test and modify an existing model for this application.

OBJECTIVES

The specific objectives of this research concerning the testing and modification of the model for monitoring soil moisture were:

1. To investigate the relationship between soil surface temperature differences and soil moisture differences as predicted by the existing heat flow model.

2. To investigate the relationship between surface soil heat flux and calculated surface temperature differences predicted by the same existing theoretical model.

3. To modify the existing heat flow model to accept plant parameters as inputs.

4. To test the modified theoretical model by comparing predicted surface temperature differences with apparent temperature difference acquired experimentally over two plots with an oats crop canopy.

BACKGROUND LITERATURE

Many previous investigations have been carried out with the over-all objective of monitoring soil moisture and underground water using thermal emittance. Myers and Heilman (1969) using pre-dawn TIR imagery found higher soil surface temperatures corresponded to soil with higher moisture content in the top 50-cm layer of soil. The possibility of employing thermography from aircraft altitudes for mapping shallow aquifers in eastern South Dakota was investigated by Myers and Moore (1972). They obtained statistically significant results for predicting the thickness of saturated sands and gravels using August predawn flight data. Thermal responses to climatic variations were found to be depicted in seasonal and diurnal thermography in a further study by Moore and Myers (1972). They concluded land use, soil moisture, and other sources of thermal differences on the land surface of the earth were easily observed using daytime thermography. They also found the effects of these variables were diminished for predawn thermography and concluded predawn flights to be best suited for identifying shallow aquifers in South Dakota.

Investigators have also explored the relationship between thermal emittance gathered at aircraft heights and soil temperature. Schmugge et al. (1978) and Reginato et al. (1976) have both shown bare soil temperatures derived from remotely sensed thermal emittance data agree with ground based soil temperatures measured using thermocouples. Tunheim (1977) showed a positive correlation between temperature patterns on the soil surface caused by near surface water

tables associated with saline seeps and airborne thermal infrared images of the same area. The results of the study also indicated that a purely heat conduction model must be modified to include other factors such as soil moisture.

Thermal inertia, the resistance of a material to a change in temperature, has also been employed to relate soil temperature to soil moisture and soil temperature to geologic formations. Schmugge et al. (1978) found the amplitude of the diurnal soil surface temperature variation, measured by airborne thermal infrared sensor, was related to soil moisture content. They also found that a greater diurnal soil surface temperature amplitude corresponded to soil with lower thermal inertia. Gillespie and Kahle (1977) collected thermal emittance data at aircraft altitude to estimate thermal inertia of the soil surface. The resultant data was used to construct a map of thermal inertia patterns on the soil surface. They then identified near surface geological formations from the map.

The first evaluation and analysis of satellite thermography data from Skylab showed positive correlation between soil moisture and thermal emittance (Moore et al., 1975). Analysis of the Heat Capacity Mapping Mission (HCMM) satellite data by Heilman and Moore (1981) showed areas of high moisture content could be detected using satellite thermal infrared imagery. However, variations of conditions at the surface and in the atmosphere must also be accounted for during analysis.

The effects of crop cover on the surface thermal emittance has been studied by several investigators. Blad and Rosenberg (1976) found the thermal emittance of the soil even at full plant cover can affect the remote temperature measurements of crop canopies. Heilman and Moore (1980) measured the thermal emittance of the soil surface partially covered by an oat crop and compared it to the thermal emittance of the crop canopy alone. They found the temperature of the partially covered soil surface to be from 0.5 C° to 11.5 C° warmer than the canopy temperature.

Quantitative measurement of soil moisture using thermal emittance would require a model that describes and simulates the effect of subsurface soil moisture on the soil surface temperature. No such model exists, although similar types of models have been developed. Kahle et al. (1975) developed a model relating daily variations in surface temperature to the thermal inertia of geologic materials. This model primarily consists of a finite difference solution to a one dimensional heat transfer problem. Soil moisture, however, is not considered an input of the model.

Meyer (1972) developed two models that relate surface thermal emittance to the presence of an aquifer. Both models consider two soil profiles 50-cm in thickness. Both models are also based on the assumption that a shallow aquifer would cause the temperature at the 50-cm depth to vary 1 C° to 3 C° from the temperature at the 50-cm depth of a region where no aquifer is present. Identical 50-cm thick homogenous soil profiles are considered in each model. The

50-cm depth was chosen because daily variations in temperature at that depth are small (Cartwright, 1968; Carson, 1961).

Surface soil heat flux is assumed to be constant in the first model and directed outward from the earth, simulating nighttime conditions. The initial values for the surface temperatures of both profiles were set equal. The presence of an aquifer at the 50-cm depth was simulated by a constant temperature diference, ΔT, between the two profiles. The heat transfer problem for both profiles was solved analytically, employing a finite integral transform. Analysis showed a surface temperature difference ranging from 20% to 40% of the assumed 50-cm temperature difference would develop in 9 hours. The rate of development of the surface temperature difference was also found to be dependent on only the thermal diffusivity of the soil.

The surface heat flux of the second model was assumed to consist of two parts, a rectified sine wave and a terrestrial radiation term as suggested by Smith (1969). It was represented in that manner in order to simulate both night and day conditions at the surface of each profile. The one dimensional heat transfer problem using this type of radiative boundary conditions could not be solved analytically. Therefore a finite difference method was chosen. Numerical calculations were carried out by computer. Calculated temperature profiles predicted from model calculations compared qualitatively with data taken by Carson (1961). One significant result that has been verified experimentally (Aaron et al., 1976) was that the maximum value for the thermal anomaly would occur at approximately 0700 hours.

The finite difference model by Meyer (1972) was further modified by Beutler (1980) to accept non-homogenous soil profiles. This non-homogeneity of soil profiles was simulated by dividing each 50-cm thick soil profile into 1-cm homogenous layers differing in bulk density, porosity and moisture content. Variations in thermal conductivity and heat capacity associated with these non-homogenous soils were thus included as factors affecting the calculated soil surface and profile temperatures.

The model by Beutler was tested by calculating surface temperature differences between a dryland and irrigated plots over a diurnal period. The calculated temperature differences were then compared to experimental data. Surface temperatures for both plots were measured using a Barnes PRT-5 radiometer. Soil temperature profiles for both plots were measured using thermocouples buried at various depths in each plot. The two soil plots were first covered by a mature barley crop. The barley crop was then stripped from both soil plots. Data were collected for both crop cover and bare soil surface conditions. Soil moisture as well as other factors were periodically monitored.

Theoretical model predictions of apparent temperature difference of the soil plots for both crop cover and bare plots were very similar functionally to the actual data. The primary difference was the absence of an experimental temperature difference during the nighttime hours for the crop covered plots. The magnitudes of the theoretical temperature differences were smaller during daytime hours but larger during nighttime hours than experimental values for both bare soil and crop covered conditions.

THEORETICAL MODEL

The finite difference heat flow model originally developed by Meyer (1972) and modified by Beutler (1980) was the model chosen for further testing and modification in the research. It uses two non-homogenous soil profiles of 50-cm depth. The 50-cm profile was chosen since daily variations in soil temperature at this depth have been observed to be small (Cartwright, 1968; Carson, 1961). The 50-cm soil profiles are then each divided into 1-cm homogenous sections or layers containing 50 equally spaced points referred to as nodal points. A diagram of this soil profile construction is illustrated in Figure 1.
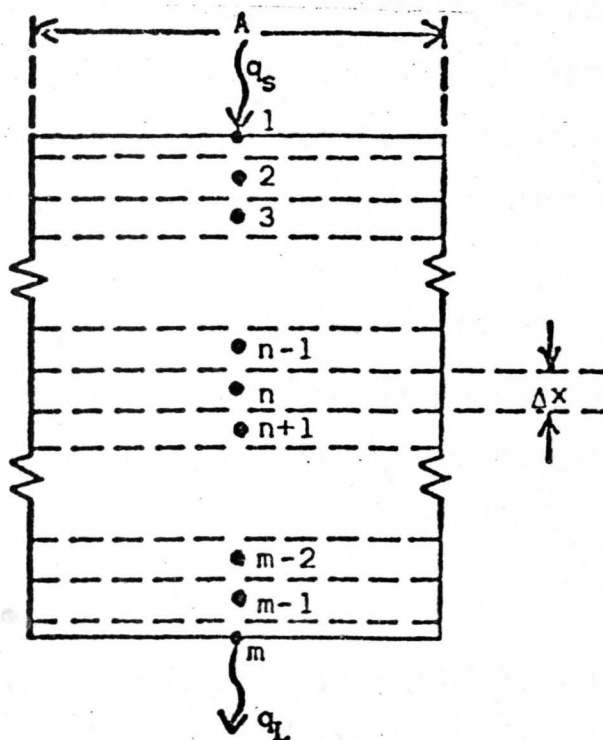
Figure 1.   Assignment of Nodal Points and Heat Flux Terms for the Finite Difference Model.

Nodal point 1 coincides with the upper surface of the soil profile at x = 0. Nodal point 50 coincides with the lower surface at x = 50. The heat flux entering the upper surface is denoted q_s while the heat flux leaving the lower surface is denoted q_L.

The heat flux q_s is difficult to measure and is thus treated as a parameter in the model. This parameter originally was composed of a rectified sine wave representing the amplitude of the solar term and a terrestrial blackbody radiation term. The original functional form of q_s is given as

$$q_s = A \sin \frac{\pi t}{L} - R, \tag{1}$$

where A is the amplitude of the solar term during the period of maximum solar radiation during one diurnal cycle, t represents the time of day measured from sunrise, L represents the total number of daylight hours, and R is the terrestrial radiation term as suggested by Smith (1969).

The model by Beutler (1980) was modified during this research to account for the shading effect of a row crop canopy on the soil surface. The soil surface heat flux term q_s was thus modified and was chosen to be of the form,

$$q_s = F_\beta A \frac{\pi t}{L} - R, \tag{2}$$

where F_β represents the fraction of field in direct sunlight and the subscript denotes the solar altitude angle at time t. The fraction of field in direct sunlight, F_β, is calculated using a model by Mann et al. (1978). This model approximates the light penetration of a

row crop incorporating both individual plant geometry and row struc-
ture. The individual plant geometry is assumed ellipsoidal as shown
in Figure 2 with vertical axis of summetry. The lengths of the semi-
major axis and semiminor axis are a' and b' respectively. The soil
surface is assumed to be horizontal. The geometrical projection of
an ellipsoid onto a horizontal surface must then be considered. The
direction of the plant projection and the solar ray are parallel.
The projection onto the soil surface is an ellipse with semimajor
axis length given by

$$a = [(b')^2 + (a' \cot \beta)^2]^{\frac{1}{2}}, \tag{3}$$

and a semiminor axis length equal to

$$b = b'. \tag{4}$$

The area of each projection is given by the equation

$$A_\beta = \pi ab, \tag{5}$$

where A_β denotes the area at solar altitude angle β. The model may
be expressed in three dimensionless constants defined as follows:

$$k_1 = \frac{a'}{b'},$$

$$k_2 = \frac{1'}{b'},$$

and $\quad k_3 = [d1'b']^{-1},$

where 1' is the distance between two consecutive rows and d is the
number of plants per unit of field area. The field is now divided
into strip areas of type A and type B to simulate the difference
between the area in the plant rows and the area between those rows.
Alternate strips are thus of the same type. Any point lying in strip
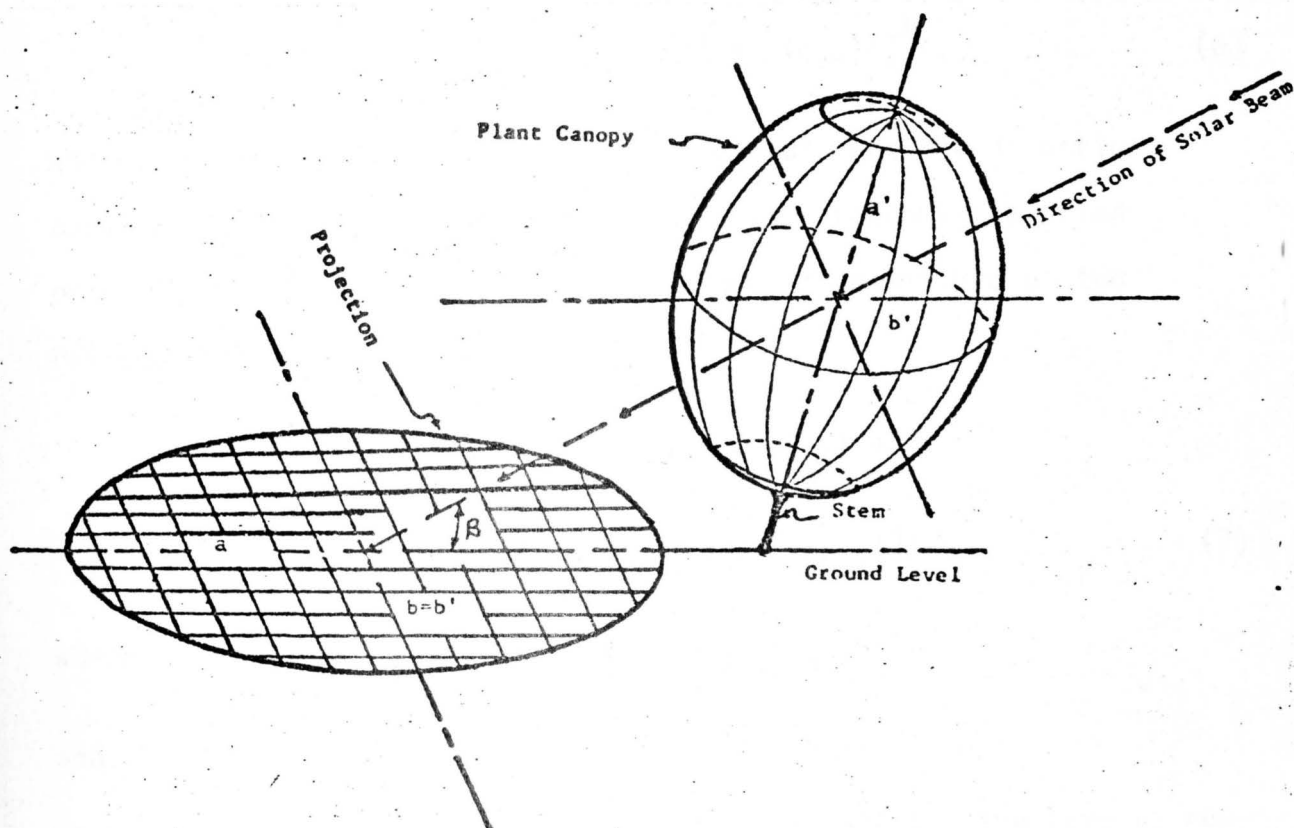
Figure 2. Ellipsoidal plant canopy and its elliptical projection
onto the soil surface (Mann et al. p 132 and Fig. 1).

type A (in the row) may be shaded by at most n-1 distinct rows. Any

point lying in strip type B may be shaded by at most n distinct rows.

This means any solar ray would have to penetrate at most n-1 rows of

plants to illuminate a point laying in a strip of type A. The value

of n is then a function of solar position and crop parameters. The

value for n is calculated employing the condition

$$n-1 \leq q \leq n,$$

where q is the ratio of the width of a canopy projection measured

perpendicularly to the rows, to the row width l'. The value for q

is calculated using the following equation;

$$q = \frac{2}{k_2} [1 + (k_1 \cot \beta \sin \alpha)^2]^{\frac{1}{2}}, \tag{6}$$

where α is the angle between the solar azimuth and the direction parallel to the rows. The probability that a randomly selected point is shaded by exactly k plant canopies is a mixture of two Poisson distributions given by;

$$P_n(k) = [\mu_n \lambda_{n,1}^k \exp(-\lambda_{n,1}) +$$

$$(1 - \mu_n)\lambda_{n,2}^k \exp(-\lambda_{n,2})]/k!, \tag{7}$$

where $\quad \mu_n = n-q; \quad \lambda_{n,1} = dA_\beta \Theta_n/\mu_n;$

and $\quad \lambda_{n,2} = dA_\beta(1 - \Theta_n)/(1 - \mu_n).$

The various terms are defined in the following text. The term μ_n represents the fractional field area which lies in strips of type A; whereas, $1 - \mu_n$ represents the fractional field area which lies in strips of type B. The term Θ_n is the fraction of a single plant canopy projection which lies in strips of type A; whereas, $1 - \Theta_n$ is the fraction of a single plant canopy projection which lays in strips of type B. The value of Θ_n is determined from the condition

$$\Theta_n = \begin{cases} 0 & , n = 1 \\ (\frac{2}{\pi}) \sum_{i=1}^{n-1} \text{Arcsin} (\frac{2i}{q} - 1) \end{cases}$$

$$+ (\frac{2i}{q} - 1)[1 - (\frac{2i}{q} - 1)^2], n > 1.$$

The term $\lambda_{n,1}$ represents the total area of all plant canopy projections which fall into strips of type A per unit of field area of

type A. The term $\lambda_{n,2}$ represents the total field area of all plant canopy projections which fall into strips of type B per unit of field area of type B.

It is assumed that the projected leaf area density of k plant canopies is the sum of the individual canopy projections. The total projected leaf area onto the soil surface is

$$c = \sum_{k=0}^{\infty} k(\frac{c'}{A})A_k , \qquad (8)$$

where c' is the total leaf area of one canopy project, A_k is the total field area shielded from the sun by k plant canopies, and A is the total field area. Equation (7) may be rewritten

$$c = \sum_{k=0}^{\infty} kc'[P_n(k)A/P_n(1)A], \qquad (9)$$

where $P_n(1)$ is the probability that a randomly selected point is shielded by exactly one plant canopy. Equation (9) may then be rewritten as

$$c = \frac{c'}{P_n(1)} \sum_{k=0}^{\infty} k\, P_n(k). \qquad (10)$$

The summation in equation (10) is the expected value of the mixture of two Poisson distributions and thus can be rewritten as

$$\sum_{k=0}^{\infty} k\, P_n(k) = \mu_n\lambda_{n,1} + (1-\mu_n)\lambda_{n,2} \qquad (11)$$

but

$$\mu_n\lambda_{n,1} + (1-\mu_n)\lambda_{n,2} = dA_\beta \qquad (12)$$

therefore substituting equation (12) into (11) yields the result

$$\sum_{k=0}^{\infty} k\, P_n(k) = dA_\beta . \qquad (13)$$

Substituting equation (13) into equation (10) yields

$$c = \frac{c'dA_\beta}{P_n(1)} .$$
(14)

The value of c is generated using the following method. The individual plant leaves are assumed to be part heliotropic and part to maintain a constant orientation with respect to the soil surface. The total projected leaf area c is a combination of these two structural characteristics. Let $R(\alpha_i)$ be the total leaf area inclined at angle α_i with respect to the horizontal plane or soil surface. The projection $c(\alpha_i,\beta)$ of $R(\alpha_i)$ onto the soil surface in the direction of the solar ray is

$$c(\alpha_i,\beta) = \begin{cases} R(\alpha_i) \cos\alpha_i & , \quad 0 < \alpha_i \leq \beta \\ R(\alpha_i)\cos\alpha_i[1 + 2(\tan\theta-\theta)/\pi], & \beta < \alpha_i; < \frac{\pi}{2} \\ R(\alpha_i)(2/\pi) \cot\beta & , \quad \alpha_i = \frac{\pi}{2} . \end{cases}$$
(15)

where $\theta = \cos^{-1}(\tan\beta \cot\alpha_i)$, (Wilson, 1967). The heliotropic portion of the canopy is assumed to maintain a fixed angle ν with respect to the solar position. The projection of this portion of the canopy, H, onto the soil surface is calculated using the expression

$$c_\nu = H \sin\nu/\sin\beta .$$
(16)

The expression for c is then rewritten as a combination of equations (15) and (16), thus

$$c = c_\nu(\beta) + \sum_i c(\alpha_i,\beta) .$$
(17)

Now assume the leaf area projected onto the area of field shielded by k plant canopies follows a random rectangular distribution

for $k = 0, 1, \cdots$. This assumption is made to simplify the calculation and make use of Beer's law to calculate the fraction of R_k which is in direct sunlight. The ratio of the projected leaf area of one canopy to the total area of all plant canopy projections is

$$c/dA_\beta A .$$

The ratio of the total projected leaf area of all plant canopy projections is

$$kc/dA_\beta A .$$

Employing Beer's law, an expression representing the fraction of R_k in direct sunlight is derived and is given by

$$F_{\beta,k} = \exp(-\frac{kc}{dA_\beta A}) . \tag{18}$$

The fraction of the entire field that is in direct sunlight is given by the weighted sum

$$F_\beta = \sum_{k=0}^{\infty} P_n(k) \exp(-\frac{kc}{dA_\beta A}) \tag{19}$$

Substituting equation (7) into equation (19) yield the equation

$$F_\beta = \mu_n \exp(-z\lambda_{n,1}) + (1-\mu_n)\exp(-z\lambda_{n,2}),$$

where $z = 1 - \exp(-\frac{c}{dA_\beta A})$. $\tag{20}$

The expression for F_β has now been derived.

The model by Beutler was further modified. The terrestrial blackbody radiation term as suggested by Fleagle (1950) originally represented the unobstructed radiation of heat from the earth toward the atmosphere. When a crop cover is present the heat radiated from the earth is obstructed by the crop canopy. The obstructed radiation

term by Fleagle (1950) is then used to describe the heat lost by each crop covered profile at night. The expression for this radiation term is

$$R = \sigma T^4 - r\sigma T_1^4 - (1-r)(.65)\sigma T_a^4 , \tag{21}$$

where σ is the Stefan-Boltzman constant, T is the temperature of the soil surface, in degrees Kelvin, T_a is the effective air temperature, in degrees Kelvin, T_1 is the temperature of the obstructing surface, in degrees Kelvin, and r represents the ratio of the obstructed area to the total area of a hemisphere circumscribed above the radiating point on the soil surface. The value of r can be shown by integration over the surface of a hemisphere to equal

$$r = \sin \Theta, \tag{22}$$

where Θ is the mean elevation angle of the tallest obstruction taken through 2π of azimuth.

Beutler (1980) modified the model by Meyer (1972) to accept non-homogenous soil profiles, as stated previously, using the following method. Consider two soil profiles identical in all respects except moisture content. If the percent soil moisture, by volume ϕ_{vw}, and the percent soil, by volume, ϕ_{vs}, are known the percent air, E_a, can be calculated. With these values known, thermal conductivity and heat capacity can be found for each one-cm thick layer in the following manner. Heat capacity for a given volume of soil is found using the following equation

$$c = \phi_{vw}c_w + \phi_{vs}c_s + \phi_{va}c_a , \tag{23}$$

where c_w, c_s, and c_a represent the heat capacities of water, soil, and

air respectively. Since c_a is small compared to c_w and c_s its effect on heat capacity is very small and is neglected. If the moisture content of the soil profile varies with depth, variations in heat capacities and thermal conductivities occur. To approximate this condition the model was constructed to accept experimental soil moisture values at several depths. The values for soil moisture over the entire 50-cm profile are then calculated and assigned by interpolation and extrapolation. Thermal conductivity is then calculated employing the method by DeVries (1963). Calculation of an apparent thermal conductivity which approximates heat transfer due to mass movement of water, phase change of water, convection, and conduction is accomplished using this method. The apparent thermal conductivity of a granular material is given by

$$\Omega = \frac{\sum\limits_{i} k_i \, x_i \, \Omega_i}{\sum\limits_{i} x_i \, \Omega_i} , \tag{24}$$

where Ω_i is the apparent thermal conductivity of the individual soil components, x_i is the volume fraction occupied by each soil component, and k_i is the ratio of the average temperature gradient in the granules across the medium. The equation for calculating a value for k_i is given by

$$k_i = 1/3 \sum_{i} [1 + (\frac{\Omega_i}{\Omega_0} - 1)g_a]^{-1} . \tag{25}$$

the values g_a are generated using an unsaturated soil, with water as the continuous medium from the equation

$$g_a = 0.33 - \frac{E_a}{\Sigma} (0.333 - 0.35) , \qquad (26)$$

where Σ is the soil porosity.

Now consider a volume of material surrounding node n (n - 2, 3, $\cdots$, m-1) as shown in Figure 3. The volume surrounding node n is given by $A\Delta x$, where A is the unit surface area and Δx is the distance between consecutive nodal points. The amount of heat transferred from node n to node n+1 is denoted $q_{n,n+1}$. The heat stored within the volume is denoted $\dot{E}_{sn}$. The law of conservation of energy to node n, considering one dimensional heat transfer results in the equation

$$q_{n-1,n} = q_{n,n+1} + \dot{E}_{sn} . \qquad (27)$$
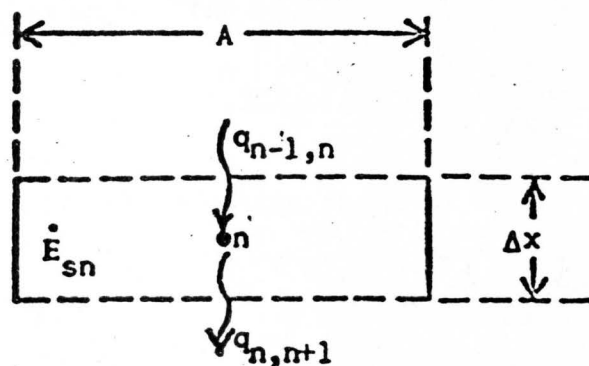
Figure 3. Energy Balance for Node n.

The rate at which heat is transferred between nodal points is written in finite difference form as

$$q_{n-1,n} = - \Omega A \frac{T_n - T_{n-1}}{\Delta x} \qquad (28)$$

and

$$q_{n,n+1} = - \Omega A \frac{T_{n+1} - T_n}{\Delta x} , \qquad (29)$$

where T_{n-1} is the temperature of node n-1, T_n is the temperature of node n, T_{n+1} is the temperature node n+1, and Ω is the thermal conductivity of the material between the nodal points. If the thermal conductivity of every volume element surrounding each nodal point is different, the thermal conductivity between nodal points may be written as the average of conductivities associated with the volume elements. Thus, for equation (29)

$$\Omega = \frac{\Omega_{n-1} + \Omega_n}{2} . \qquad (31)$$

Equation (28) may then be written as

$$q_{n-1,n} = - \left(\frac{\Omega_{n-1} + \Omega_n}{2}\right) A \frac{T_n - T_{n-1}}{\Delta x} . \qquad (32)$$

Similarly, equation (29) is rewritten as

$$q_{n,n+1} = - \left(\frac{\Omega_n + \Omega_{n+1}}{2}\right) A \frac{T_{n+1} - T_n}{\Delta x} . \qquad (33)$$

The energy storage term expresses the rate at which the temperature of the volume of material changes. This term may be written in finite difference form as

$$\dot{E}_{sn} = (\rho c)_n A \Delta x \frac{T_n' - T_n}{\Delta t} , \qquad (34)$$

where ρ is the density, c is the heat capacity, Δt is the time increment, T_n is the temperature of node n at time t, and T_n' is the temperature of node n at time t + Δt. Substituting equations (32), (33), and (34) into equation (27) and rearranging terms yields

$$\frac{T_n - T_n}{\Delta t} = \frac{1}{2(\rho c)_n (\Delta x)^2} [(\Omega_{n-1} + \Omega_n)T_{n-1} - (\Omega_{n-1} + 2K_n + k_{n+1}) T_n$$

$$+ (\Omega_n + \Omega_{n+1}) T_{n+1}] . \tag{35}$$

Solving for the temperature at time $t + \Delta t$ results in the equation

$$T_n' = \frac{(\Omega_{n-1} + \Omega_n)\Delta t}{2(\rho c)_n (\Delta x)^2} T_{n-1} + [1 - \frac{(\Omega_{n-1} + 2\Omega_n + \Omega_{n+1})\Delta t}{2(\rho c)_n (\Delta x)^2}] T_n$$

$$+ \frac{(\Omega_n + \Omega_{n+1})\Delta t}{2(\rho c)_n (\Delta x)^2} T_{n+1} . \tag{36}$$

Now consider the transfer of heat at the surface, $x = 0$. Figure 4 shows the volume element for node 1.
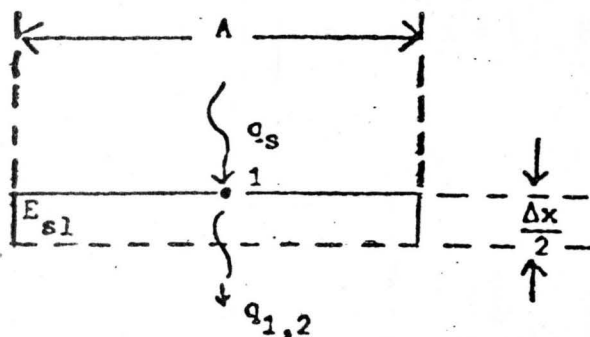
Figure 4. Energy Balance for Node 1.

The energy balance equation can be written as

$$q_s = q_{1,2} + \dot{E}_{s1} . \tag{37}$$

The rate of heat transfer from node 1 to node 2 is

$$q_{1,2} = - (\frac{\Omega_1 + \Omega_2}{2}) A \frac{T_2 - T_1}{\Delta x} . \tag{38}$$

Node 1 is at the surface, therefore, the volume of material surrounding node 1 is $(\Delta x/2)A$. The energy storage term is then

$$\dot{E}_{s1} = (\rho c)_1 A(\Delta x/2) \frac{T_1' - T_1}{\Delta t} \tag{39}$$

Substituting equations (37) and (38) into equation (39) and rearranging yields the equation

$$\frac{T_1' - T_1}{\Delta t} = \frac{2q_s}{A(\rho c)_1 \Delta x} + \frac{\Omega_1 + \Omega_2}{(\rho c)_1 (\Delta x)^2} [T_2 - T_1] . \tag{40}$$

Solving for the new temperature, T_1', gives

$$T_1' = \frac{2q_s \Delta t}{A(\rho c)_1 \Delta x} + [1 - \frac{(\Omega_1 + \Omega_2)\Delta t}{(\rho c)_1 (\Delta x)^2}] T_1 + \frac{(\Omega_1 + \Omega_2)\Delta t}{(\rho c)_1 (\Delta x)^2} T_2 . \tag{41}$$

Finally, consider the node at the lower boundary, $x = L$. Figure 5 depicts the volume element for node m.
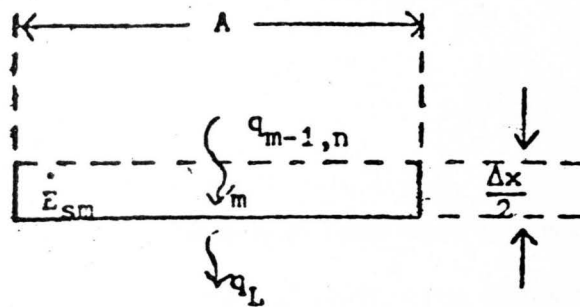
Figure 5. Energy Balance for Node m.

The energy balance equation for node m is given by the equation

$$q_{m-1,m} = q_L + \dot{E}_{sm} . \tag{42}$$

The rate of heat transfer from node m-1 to node m is represented by the equation

$$q_{m-1,m} = - (\frac{\Omega_{m-1} + \Omega_m}{2})A \frac{T_m - T_{m-1}}{\Delta x} . \tag{43}$$

Once more, since the volume element surrounding node m is only $(\Delta x/2)A$, the energy storage term can be written as

$$\dot{E}_{sm} = (\rho c)_m A(\frac{\Delta x}{2}) \frac{T_m' - T_m}{\Delta t} . \tag{44}$$

Substituting equations (42) and (43) into equation (44) and rearranging, results in the equation

$$\frac{T_m' - T_m}{\Delta t} = \frac{\Omega_{m-1} + \Omega_m}{(\rho c)_m (\Delta x)^2} T_{m-1} - T_m - \frac{2q_L}{A(\rho c)_m \Delta x} . \tag{45}$$

Solving for the new temperature T_m' yields the equation

$$T_m' = \frac{(\Omega_{m-1} + \Omega_m)\Delta t}{(\rho c)_m (\Delta x)^2} T_{m-1} + [1 - \frac{(\Omega_{m-1} + \Omega_m)\Delta t}{(\rho c)_m (\Delta x)^2}] T_m$$

$$- \frac{2q_L \Delta t}{(\rho c)_m A \Delta x} . \tag{46}$$

The finite difference equations have now been derived and are equations (36), (41), and (46). The solution of a one-dimensional heat transfer problem requires the specification of an initial temperature for each of the m nodel points. The method described is an analytically solved problem using a specified initial condition. To calculate the new temperature at time Δt the heat flux terms q_s to q_L must be specified. Equations (41) and (46) may then be used to determine the new boundary temperatures. The new temperature of each

interior nodal point can be determined by solving equation (36) for each node n (n = 2, 3 ... m-1). The resultant temperatures obtained for the m nodal points can then be used to calculate the temperatures at time 2Δt. The iteration process is then continued to obtain the temperature of any nodal point at any desired future time.

Choice of values of Δx and Δt depends on the thermal properties of the soil considered and the thickness of the soil layer. The values Δt = 60 seconds and Δx = 1-cm were found to be sufficient (Beutler, 1980) for a 50-cm soil layer and the range of soil thermal properties used.

The finite difference model (Figure 6) requires the following inputs: (1) crop parameters, (2) soil heat flux, (3) soil moisture profile, (4) dry soil conductivity, (5) physical parameters of the soil which include the bulk density and the amount of soil by volume, (6) initial temperature profile, and effective air temperature.

Outputs of model calculations, are soil temperature profiles, for the two sites, and a surface temperature difference between the two soil plots as a function of time.
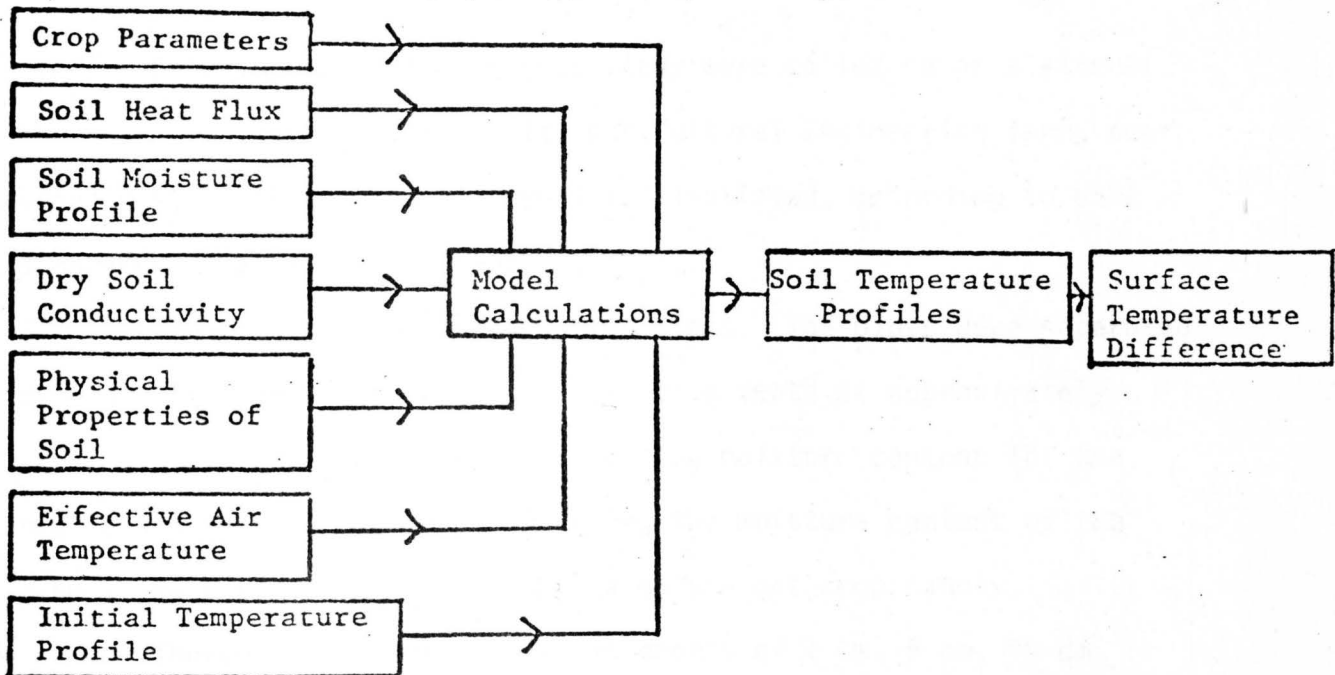
Figure 6. Schematic representation of the finite-difference model in its present format.

DATA COLLECTION

Experimental data for this study were collected on a site at the South Dakota State University Agricultural Engineering farm, near Brookings, South Dakota. The soil is classified, according to USDA standards as a silt loam (Beutler, 1980).

The site was divided into two plots. The plots were separated by a plastic water vapor barrier down to a depth of approximately 100 cm. This was done to ensure that the moisture content for one plot could be varied without affecting the moisture content of the other. Both plots were covered by a mature oat crop canopy.

Thermocouples were buried at depths of 1 cm, 5 cm, 10 cm, 25 cm, and 50 cm. Soil profile temperatures were recorded every 30 minutes. The thermal emittance of the soil and crop canopy was measured using a Barnes PRT-5 mounted on an apparatus which allowed the scanning of both plots at 30 minute intervals from a height of approximately 3 m above the soil surface. Wet bulb and dry bulb air temperature data were collected every hour. Solar radiation and net-solar radiation data were collected every 30 minutes.

Soil moisture by weight was acquired using the gravimetric method with collection of soil samples during midmorning and again during the early evening hours. Soil samples for these measurements were collected on the surface, at a 1 cm-8 cm depth, at a 8 cm-25 cm depth and at a 25 cm-50 cm depth. Soil moisture by volume was then obtained in each case by multiplying soil moisture by weight by the average bulk density of the soil for each depth.

Crop parameters were estimated by measurement of plant height, width and row spacings. The values for these parameters do not represent a statistical study of each parameter value.

RESULTS

This research consists of two parts. The first part is an investigation using the theoretical model by Beutler (1980) to obtain a relationship between soil moisture difference and the maximum surface temperature difference observed during a diurnal cycle for two soil plots. The second consists of a modification of the model to accept crop parameters as inputs and subsequent testing of the modified model by comparing predicted surface temperature differences between two soil plots with experimental data.

Near-surface soil moisture and soil surface temperature have been shown by investigators to be related to one another (Idso et al., 1975, Schmugge et al., 1978). Soil surface temperature difference has also been shown to have a similar functional form as surface temperature during the diurnal cycle (Beutler, 1980). This would indicate that surface temperature difference may be a useful tool for measuring soil moisture eliminating the need for recalibration of thermal emittance data due to atmospheric and surface effects.

Several series of calculations using the original theoretical model were carried out to predict the type of relationship between soil moisture difference and maximum surface temperature difference which might be expected between two soil plots. During all calculations both plots were assumed to have no plant canopy. Values for soil heat flux and soil physical properties were chosen to correspond to experimental observations and were identical for both plots. The percent soil moisture for each individual plot was assumed constant

throughout the entire profile. The value for soil moisture of the reference plot was held constant during each series of calculations while the value for soil moisture of the other plot was varied. The surface temperature differences were calculated for each soil moisture difference as a function of time during a complete diurnal cycle. The maximum surface temperature difference during each diurnal cycle was then plotted as a function of soil moisture difference.

Results of calculations for a reference plot moisture of 5% by volume are shown in Figure 7. The temperature at the 50 cm depth was assumed equal for both soil profiles. The maximum temperature difference in all calculations were found to be positive (the dry- land plot was warmer than the irrigated plot) and occurred at approximately 1300 hours. The points shown are calculated values and the continuous curve was fitted to these values using multiple linear regression analysis. The continuous line has a quadratic functional form and is readily seen in Figure 7 to be an excellent fit.

The reference plot moisture was then increased to 10% by volume and the procedure was repeated generating a new set of maximum surface temperature differences. Calculated values were plotted again and the resultant graph is shown in Figure 8. Multiple linear regression analysis was performed and the continuous curve fitted to the calculated points. The curve again has a quadratic form and fits the calculated values very well.

The calculation procedure was repeated for a reference plot moisture of 20% by volume. The maximum temperature differences from

Figure 7. Calculated surface temperature difference between two soil plots as a function of moisture difference. One plot is considered to have a fixed soil moisture profile of 5% by volume while the other is varied from that value. The temperature difference at a depth of 50-cm is 0 C°.

Figure 8. Calculated surface temperature difference between two
soil plots as a function of moisture difference. One
plot is considered to have a fixed soil moisture
profile of 10% by volume while the other is varied
from that value. The temperature difference at a
depth of 50-cm is 0 C°.

these calculations are shown in Figure 9. The continuous curve from multiple linear regression analysis again fits these values extremely well.

Comparison of Figures 7, 8 and 9 shows the maximum surface temperature difference between the two plots decreases with increasing reference plot soil moisture. For example, a reference plot moisture of 5% and a moisture difference of 10% in Figure 7 depicts a maximum surface temperature difference of 5.8 C°. However, Figure 8 and Figure 9 depict maximum temperature differences of 4.0 C° and 2.2 C° respectively for the same moisture difference.

Results of calculations using reference moistures of 2.5%, 7.5%, and 15% by volume were also carried out but are very similar and will not be shown.

Meyer (1972) assumed the presence of a shallow aquifer would cause the soil temperature at a depth of 50-cm to be 1.0 C° to 3.0 C° cooler when compared to a non-aquifer region. Employing this assumption a series of theoretical calculations were carried out to explore the effect that a temperature difference at the 50-cm depth would have on the relationship between soil moisture difference and maximum surface temperature difference.

The calculations were carried out in precisley the same manner as before. The reference plot soil moisture values used were 2.5%, 5.0%, 7.5%, 10%, 15%, and 20%. The 50-cm temperature differences were assumed to be 0.5 C°, 1.0 C°, 1.5 C°, 2.0 C°, 2.5 C°, and 3.0 C°. The maximum temperature difference was again found to be
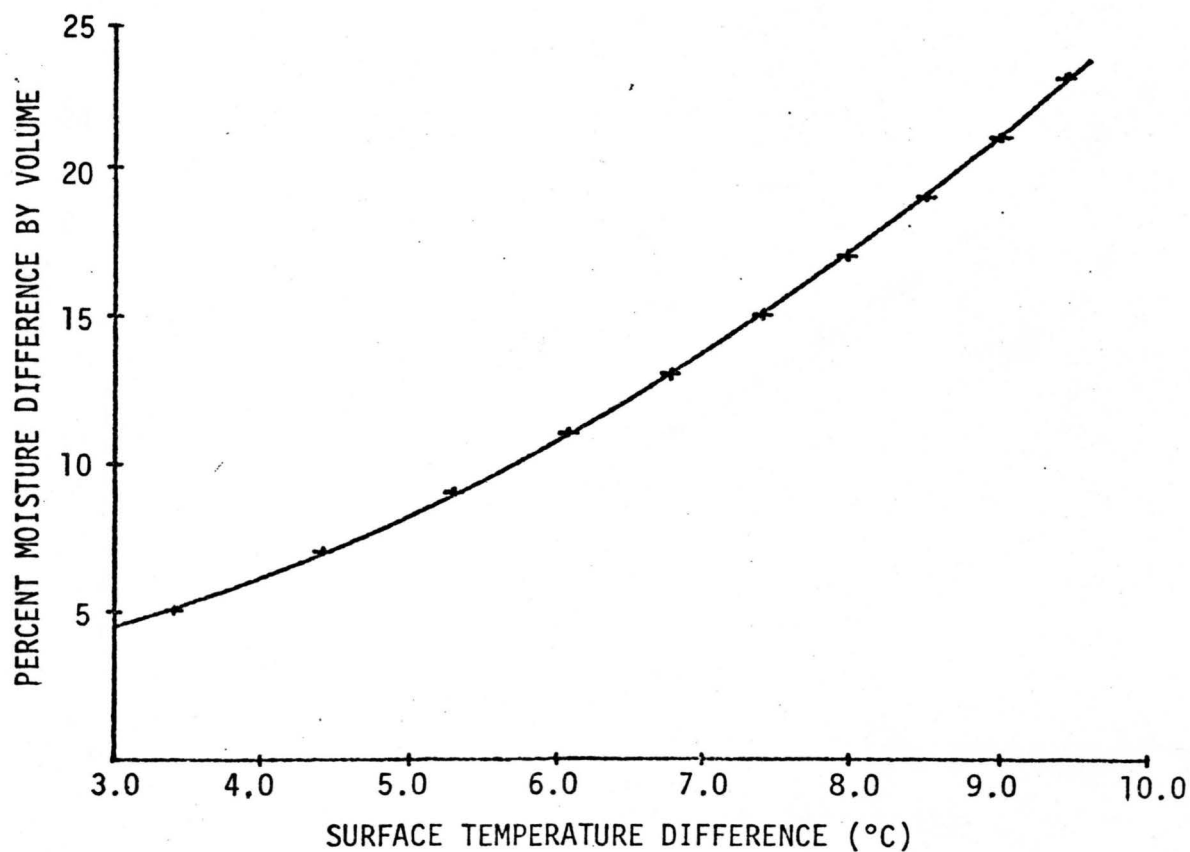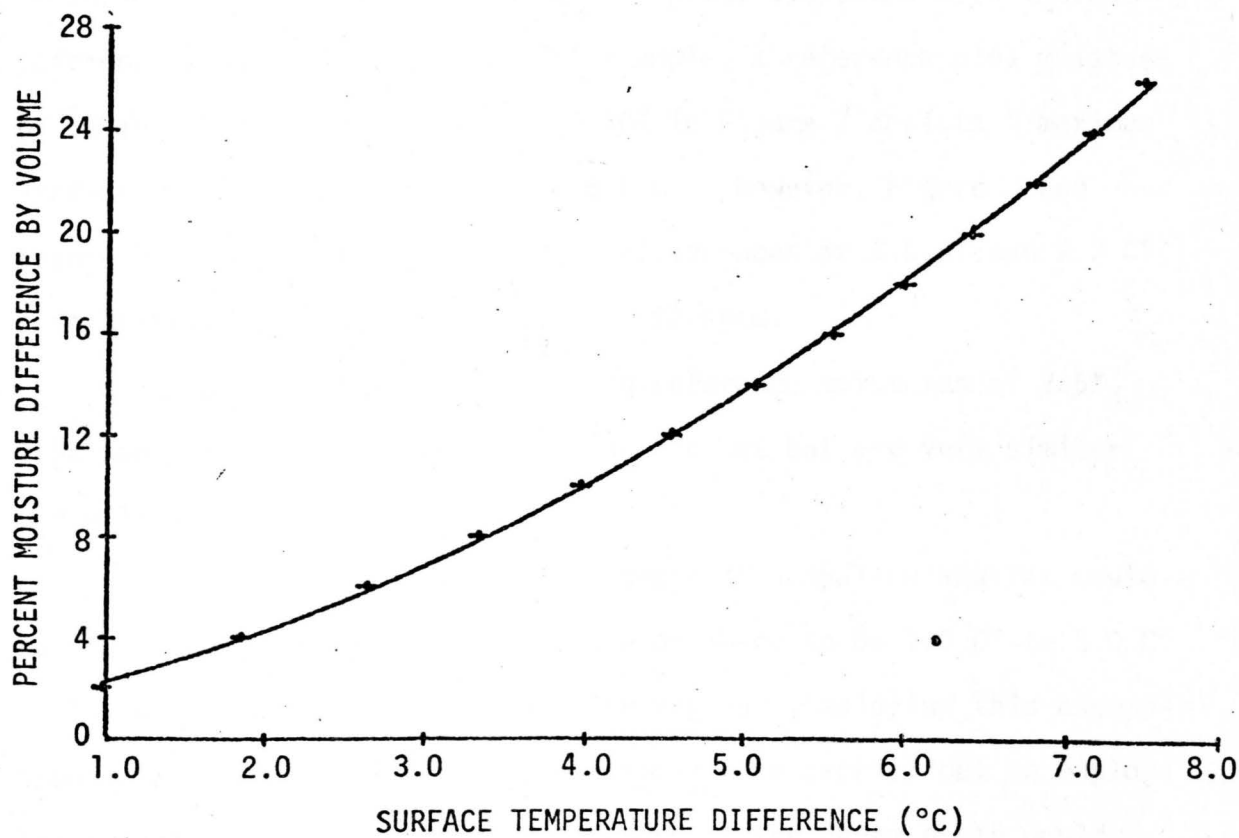
Figure 9. Calculated surface temperature difference between
two soil plots as a function of moisture difference.
One plot is considered to have a fixed soil mois-
ture profile of 20% by volume while the other is
varied from that value. The temperature difference
at a depth of 50-cm is 0 C°.

positive in all calculations and occurred at 1300 hours. Calculated values were plotted and continuous curves fit to each set of data points using multiple linear regression analysis. Results for a 1.0 C° 50-cm temperature difference and reference plot moistures of 5%, 10%, and 20% by volume are shown in Figures 10, 11, and 12 respectively. The continuous curves were quadratic in all cases and fit the data extremely well. Note also, the maximum surface temperature decreases as the reference plot soil moisture increases in the same manner as for the previous set of calculations. This trend continued for all sets of calculations completed.

A possible explanation for the decreasing maximum temperature differences with increasing reference plot moisture may be the increase in thermal inertia associated with the increasing soil moisture. Thermal inertia is the square root of the product of thermal conductivity and heat capacity. The thermal conductivity increases as does the heat capacity of the soil with increasing soil moisture at low and intermediate values of soil moisture. As the soil moisture content approaches saturation, however, the thermal conductivity and heat capacity of the soil approach constant values. Thus, as soil moisture is increased in an initially dry soil thermal inertia tends to increase rapidly but approaches a constant value at high soil moisture values.

Increasing thermal inertia has the effect of decreasing the temperature changes of the soil during a diurnal cycle. This condition has been shown to exist for soils with large moisture content

Figure 10. Calculated surface temperature differences between two soil plots as a function of moisture difference. One plot is considered to have a fixed soil moisture profile of 5% by volume while the other is varied from that value. The temperature difference at a depth of 50-cm is 1 C°.

Figure 11. Calculated surface temperature difference between two soil plots as a function of moisture difference. One plot is considered to have a fixed soil moisture profile of 10% by volume while the other is varied from that value. The temperature difference at a depth of 50-cm is 1 C°.
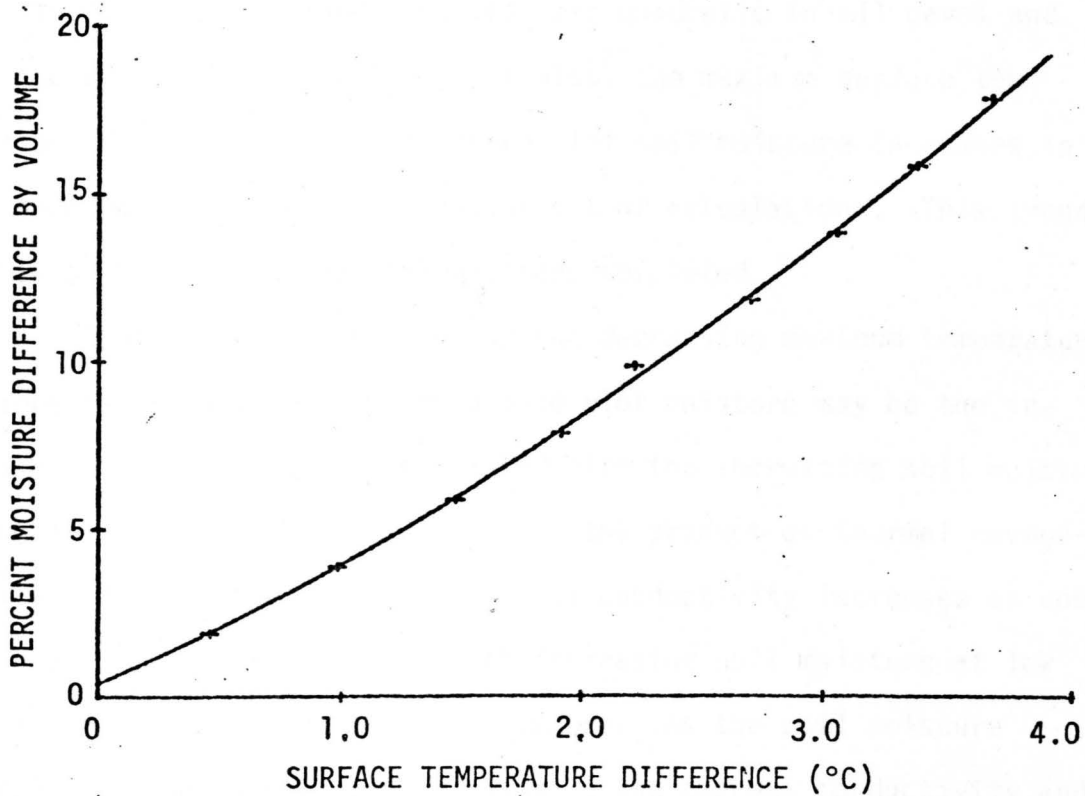
Figure 12. Calculated surface temperature difference between two soil plots as a function of moisture difference. One plot is considered to have a fixed soil moisture profile of 20% by volume while the other is varied from that value. The temperature difference at a depth of 50-cm is 1 C°.

by Beutler (1980) and Idso et al. (1975). An increase in thermal
inertia will decrease the maximum surface temperature of the soil
which occurs at 1300 hours during the diurnal cycle. Thus if soil
moisture is increased in both plots keeping the same soil moisture
difference, the maximum temperature of both plots is decreased. Thus
the maximum temperature difference between the plots will also be
decreased. This would explain the smaller maximum surface temperature
difference calculated by the model for each increase in reference plot
moisture.

Results of model calculations for a reference plot moisture
of 10% by volume and temperature differences of 2 C° and 3 C° at the
50-cm depth are shown in Figures 13 and 14. The continuous curve is
again quadratic in functional form. Comparison of Figures 8, 11, 13,
and 14 indicates the maximum temperature difference increases when
the temperature difference at the 50-cm depth is assumed to be 1 C°.
A further increase in the 50-cm temperature difference, however, does
not lead to further increase in maximum surface temperature difference.
For example, the maximum temperature difference for a moisture differ-
ence of 15% from Figure 8 is approximately 5.2 C°, whereas the same
moisture difference gives a maximum surface temperature difference
of approximately 6.2 C°, 5.8 C°, and 5.8 C° as shown in Figures 11,
13, and 14, respectively.

This result is consistent with results by Meyer (1972). Using
the original theoretical finite difference model he concluded a thermal
anomaly at a depth of 50-cm had little effect on the surface thermal
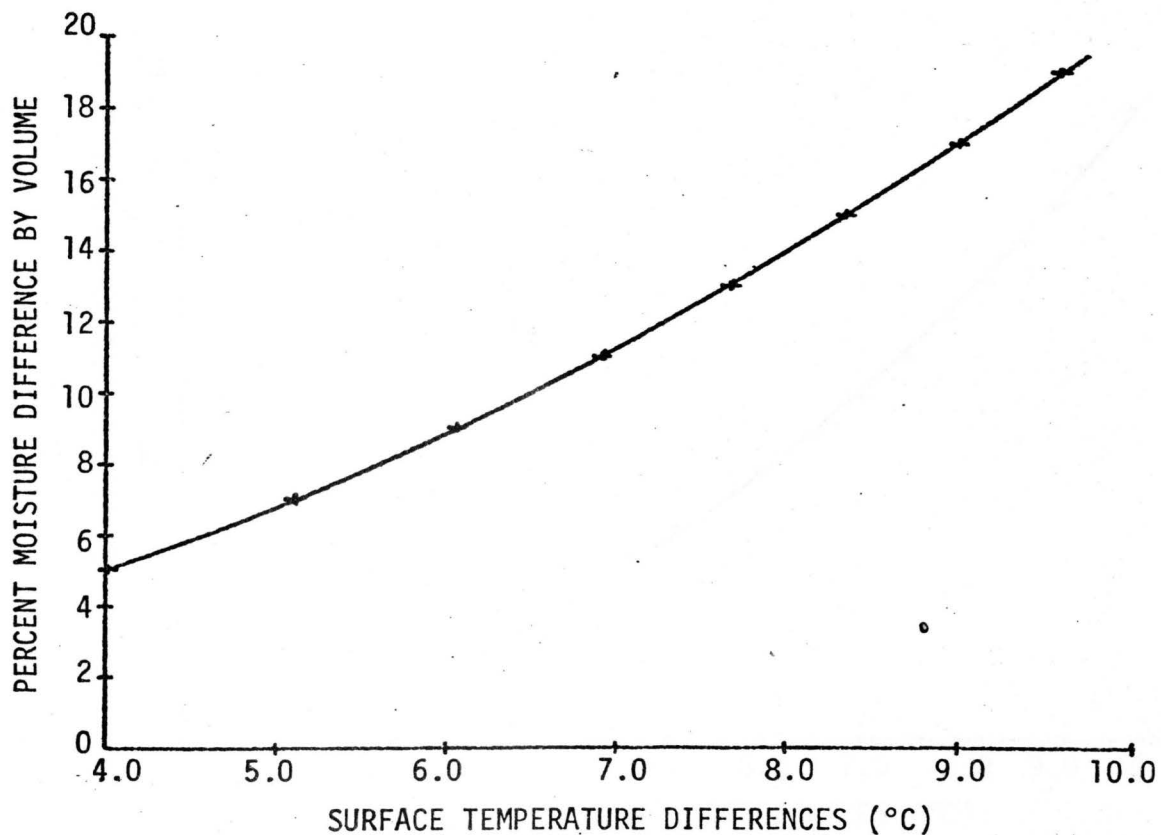anomaly during the middle of the day.
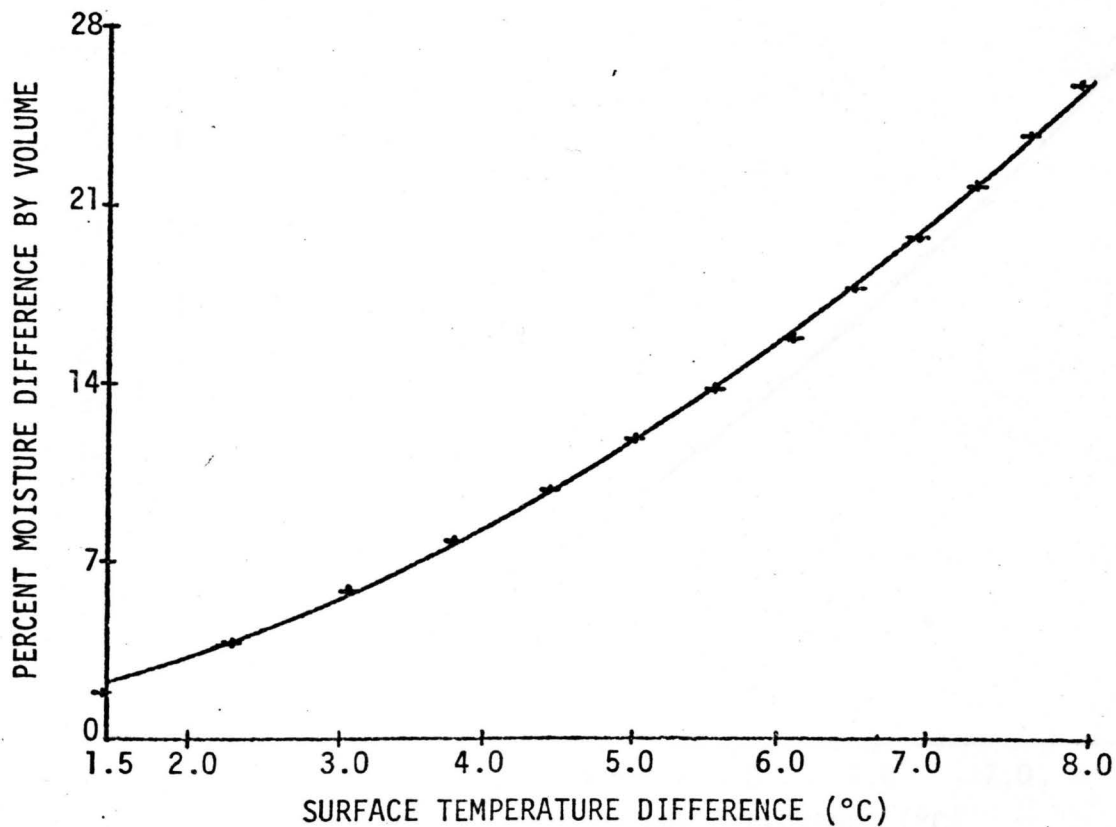
Figure 13. Calculated surface temperature difference between two soil plots as a function of moisture difference. One plot is considered to have a fixed soil moisture of 10% by volume while the other is varied from that value. The temperature difference at a depth of 50-cm is 2 C°.
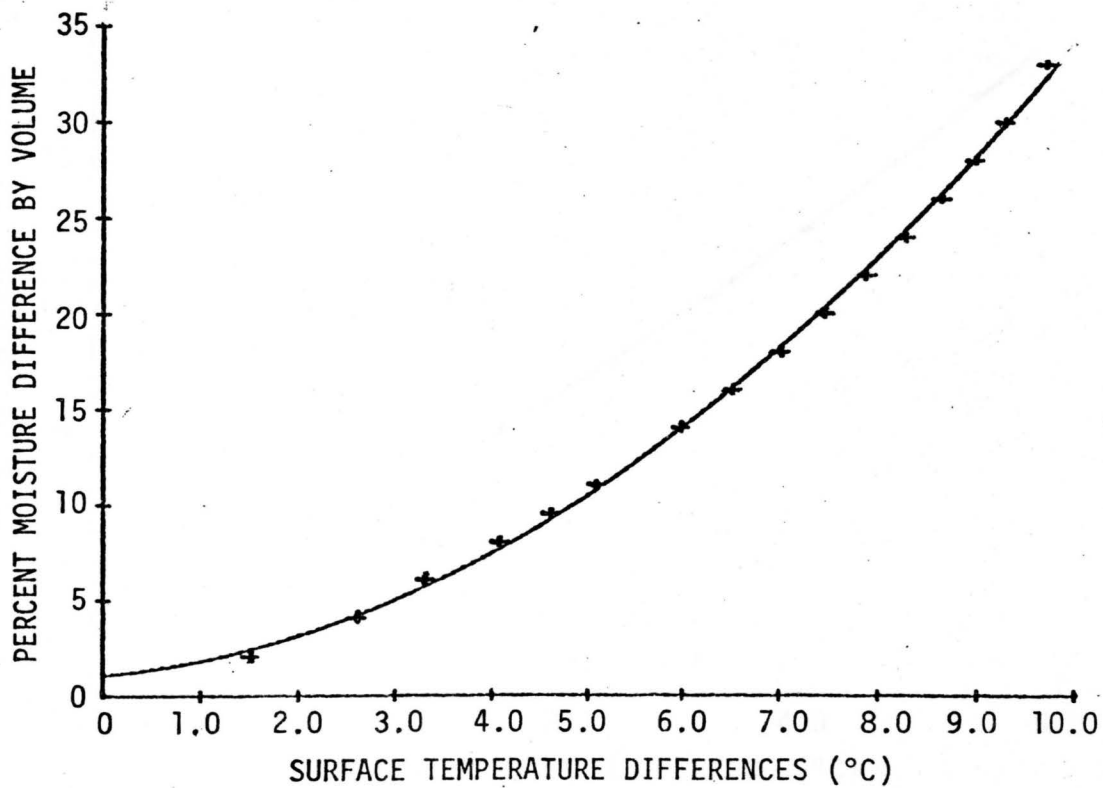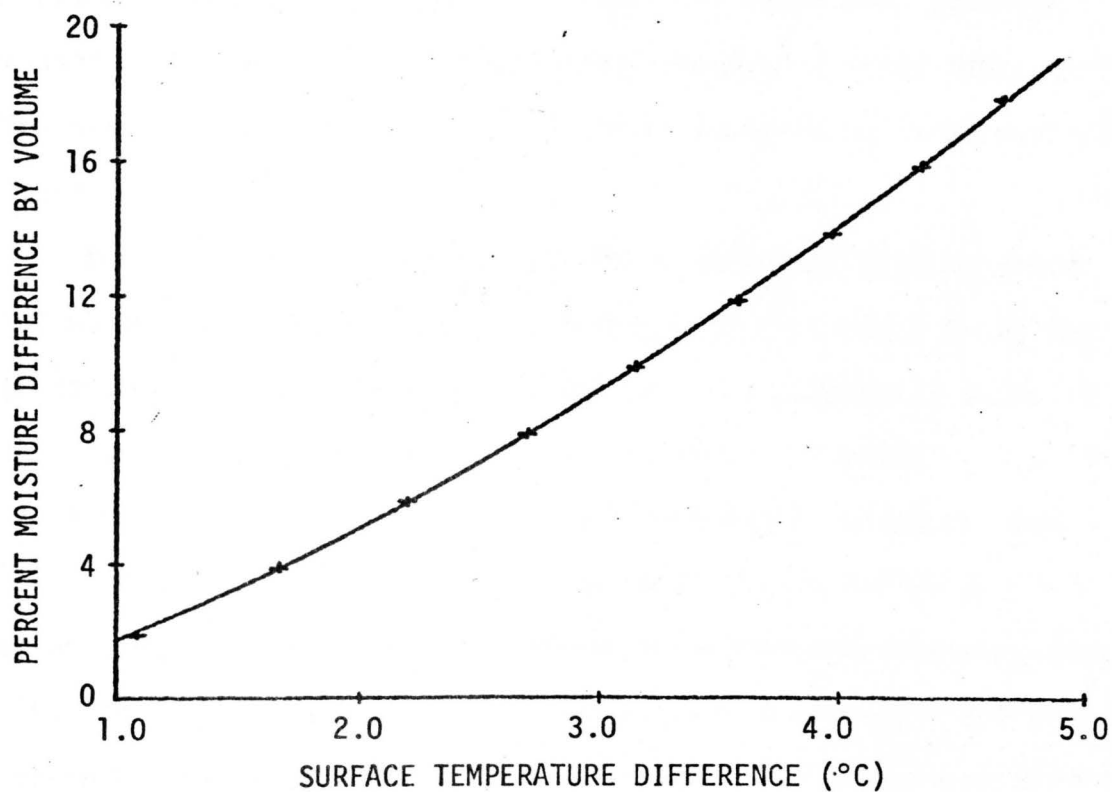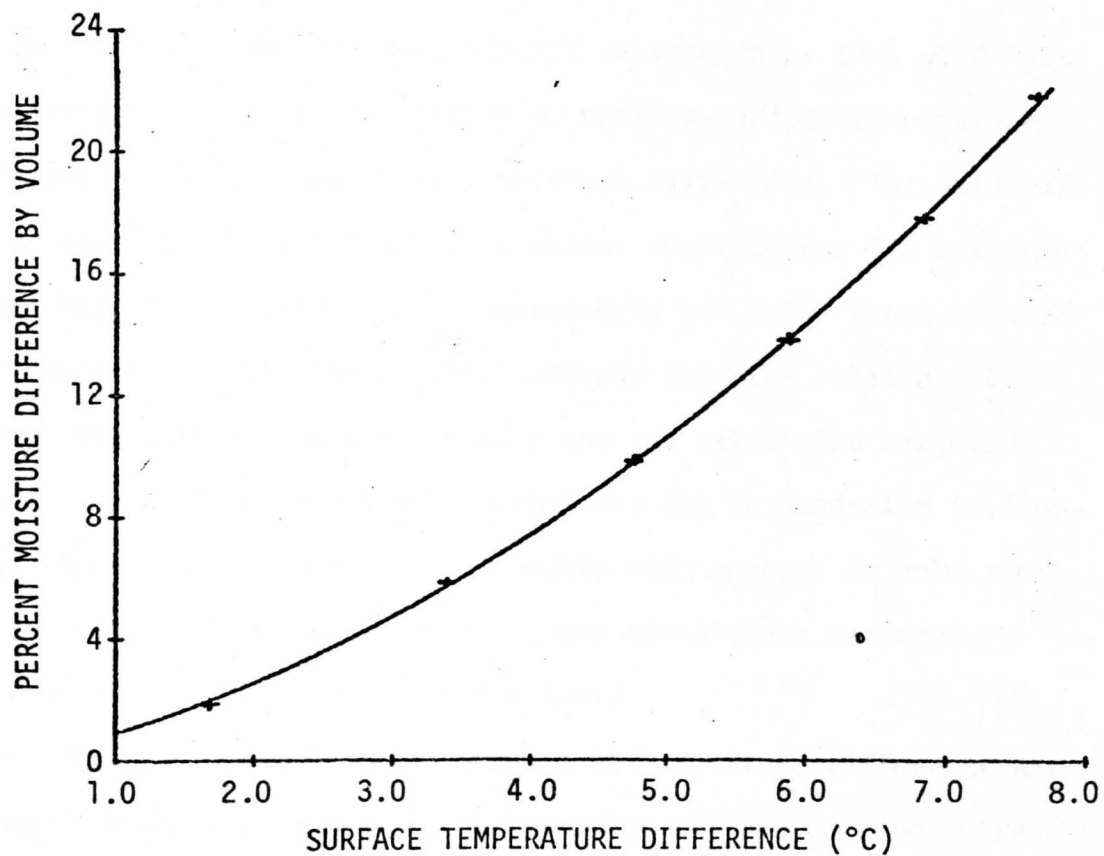
Figure 14. Calculated surface temperature difference between two soil plots as a function of moisture differ-ence. One plot is considered to have a fixed soil moisture of 10% by volume while the other is varied from that value. The temperature differ-ence at a depth of 50-cm is 3 C°.

Results for other theoretical calculations relating soil moisture difference and maximum surface temperature difference with a 50-cm soil temperature difference were similar and will not be shown.

The most significant result from these calculations using the theoretical model is the quadratic relationships. that were found to represent the calculated values of maximum surface temperature difference as a function of soil moisture difference. The value of the R^2 term for every set of calculations derived from the multiple linear regression analysis was between 0.99 and 1.0. These highly statistically significant results indicate that the relationship between the soil moisture difference and the calculated maximum temperature difference observed during the day is quadratic in functional form. The quadratic relationship also appears to hold true for all values of reference moisture and 50-cm depth temperature differences that might occur in the field.

Since the relationship between soil moisture difference and maximum surface temperature difference were all represented extremely well by quadratic equations, an attempt was made to determine possible relationships between coefficients of the equations describing these curves. The general form of these equations would be given by

$$\Delta M = A + B\ (\Delta T) + C\ (\Delta T)^2,$$

where ΔM is the % soil moisture difference between plots and ΔT is the maximum surface temperature difference during the diurnal cycle. The coefficients A, B and C will be functions of the percent soil moisture

of the reference plot. Results of a linear regression analysis for
0 C° temperature difference at the 50-cm depth are shown in Figures 15,
16, and 17. Figure 15 shows the results for the constant term A. The
points are calculated values of A as a function of reference plot soil
moisture. The continuous curve is given by

$$A = 0.0559 - 0.7126M + 2.3393M^2.$$

Where M is the reference moisture in fractional form by volume. The
quadratic relationship found between the constant A and reference
moistures is statistically significant with a R^2 value of 0.89.

Results for the linear coefficients B are shown in Figure 16.
The functional relationship between linear coefficients and reference
moistures was also found quadratic in functional form and is repre-
sented by the equation

$$B = 0.0109 + 0.2317M - 0.1209M^2$$

The relationship is statistically significant with an R^2 value of 0.97.

Figure 17 shows the results of analysis for the quadratic
coefficients C. The relationship between C and reference moisture
was again found quadratic in form and is represented by the equation

$$C = 0.0013 + 0.0201M - 0.0285M^2$$

The relationship is also statistically significant with an R^2 value
of 0.93.

Multiple linear regression analysis was performed on the data
corresponding to temperature differences of 0.5 C°, 1.0 C°, 1.5 C°,
2.0 C°, 2.5 C°, and 3.0 C° at the 50-cm depth. Results showed that
in every instance a quadratic relationship was found to be

Figure 15. Reference plot soil moisture by volume as a
function of the regression coefficient A for
a 0 C° temperature difference at a depth of
50-cm.

Figure 16. Reference plot soil moisture by volume as a function of the regression coefficient B for a 0 C° temperature difference at a depth of 50-cm.

Figure 17. Reference plot soil moisture by volume as a function of the regression coefficient C for a 0 C° temperature difference at a depth of 50-cm.

statistically significant with R^2 values of no less than 0.82. An example of results for the analysis with a 3 C° temperature difference at the 50-cm depth are shown in Figures 18, 19, and 20.

It should be noted from Figures 15 thru 20 that the two reference moisture values, which are difficult to fit to the quadratic equation are the 0.025 and 0.20 values. These represent the extremely dry and the wet soil situations. A similar problem was found for all results. This situation may be explained using results of a study comparing soil heat flux predicted from DeVries (1963) and experimental data by Kimball et al. (1975). Kimball et al. (1975) found the DeVries method to predict soil thermal conductivity well only at intermediate soil moisture contents. Thus, the coefficients associated with reference moistures of 0.025 and 0.20 by volume may possibly be expected to give poorer statistical results.

If further theoretical and experimental investigation results in a valid quadratic relationship between regression coefficients and a reference moisture, a method for measuring soil moisture over large areas of the earth would be greatly simplified. This technique would require the ground truth monitoring of soil moisture at a reference site and acquisition of satellite thermal emittance data. The appropriate coefficients could be calculated from the reference soil moisture and an appropriate quadratic function relating moisture difference could then be generated. Using this function the soil moisture of any other site could then be determined.
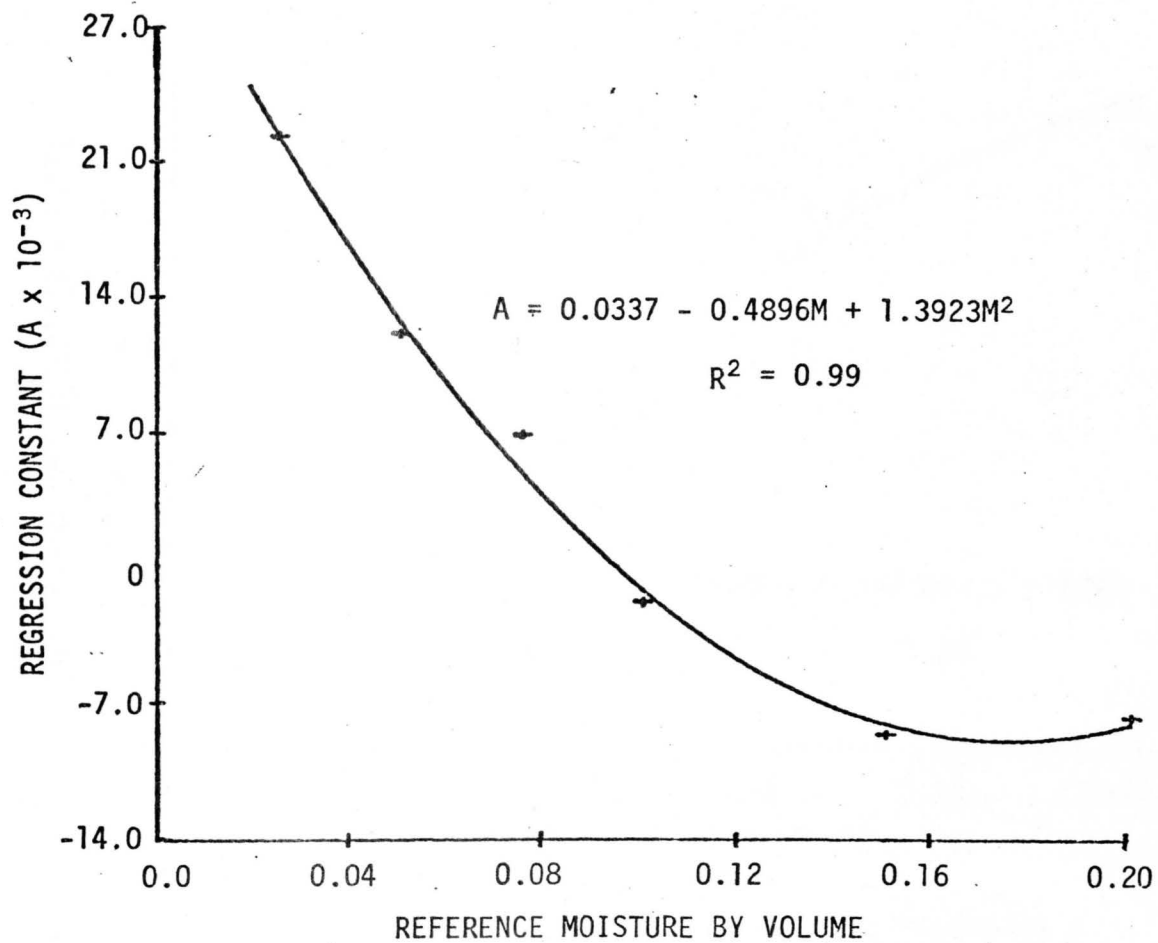
Figure 18. Reference plot soil moisture by volume as a function of the regression coefficient A for a 3 C° temperature difference at a depth of 50-cm.
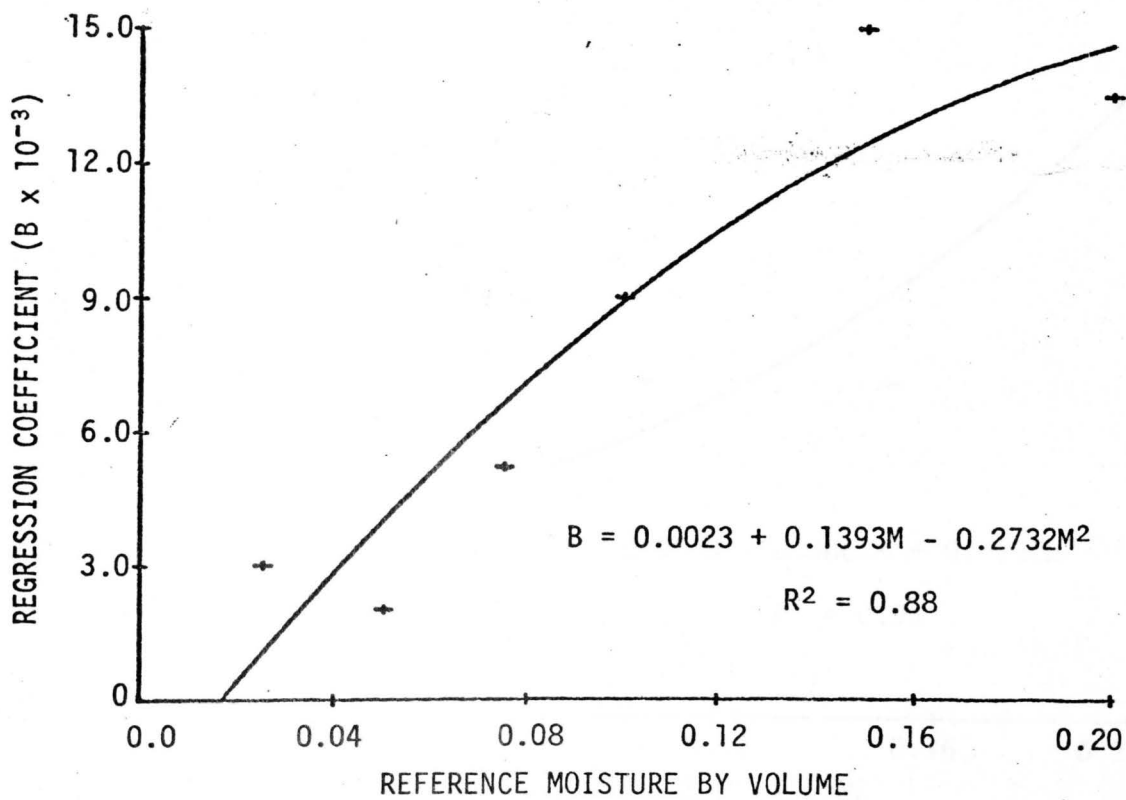
Figure 19. Reference plot soil moisture by volume as a function of the regression coefficient B for a 3 C° temperature difference at a depth of 50-cm.
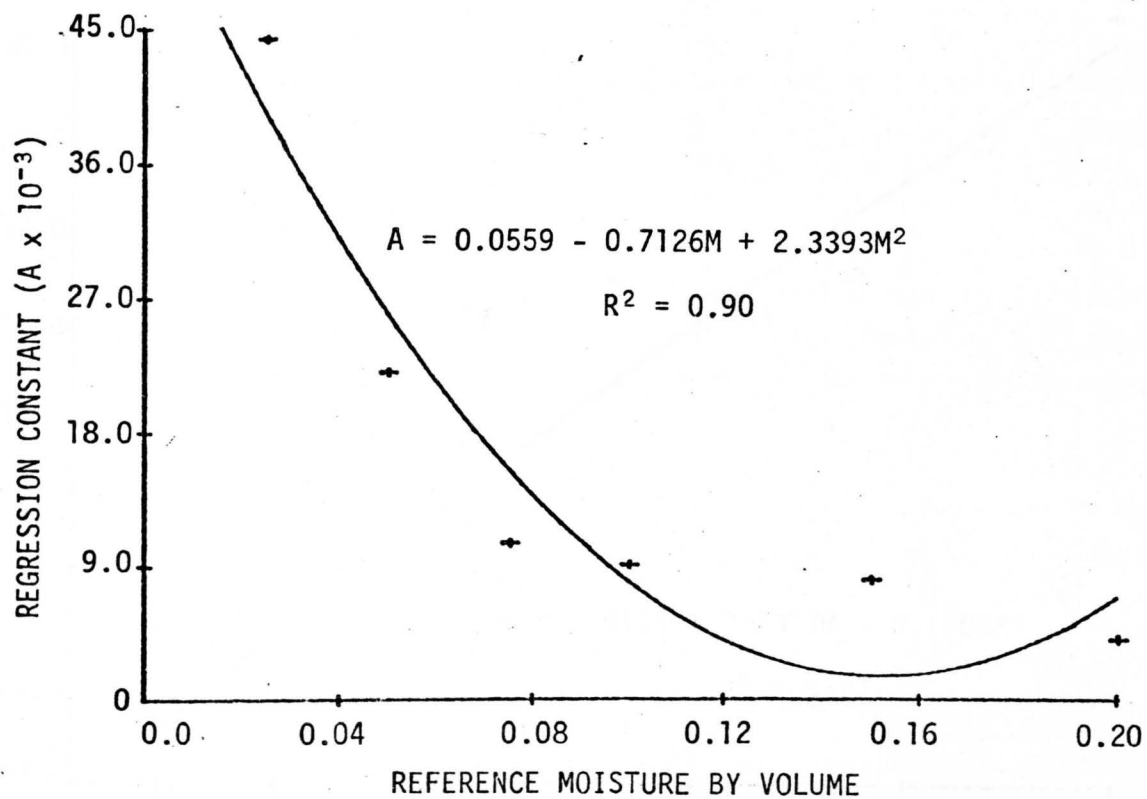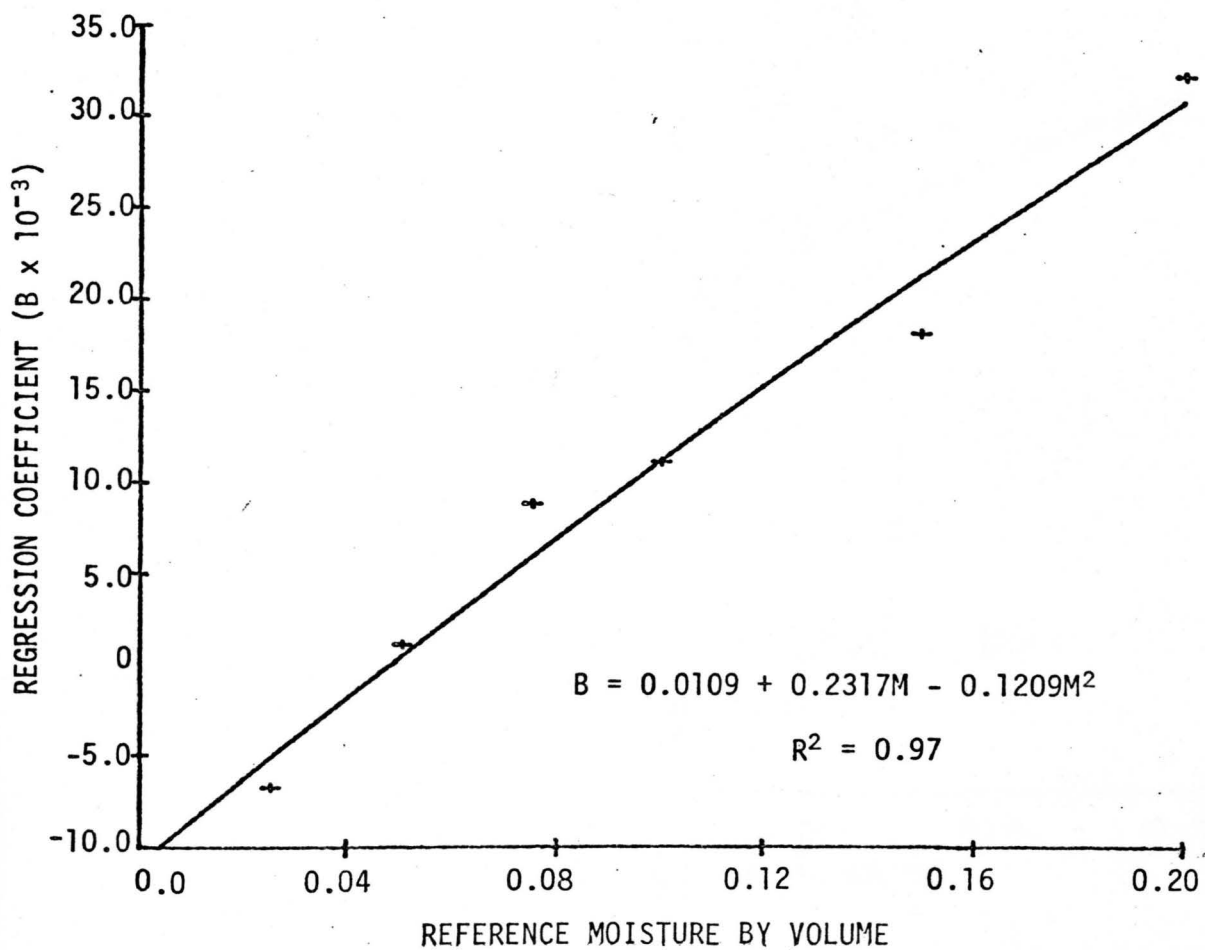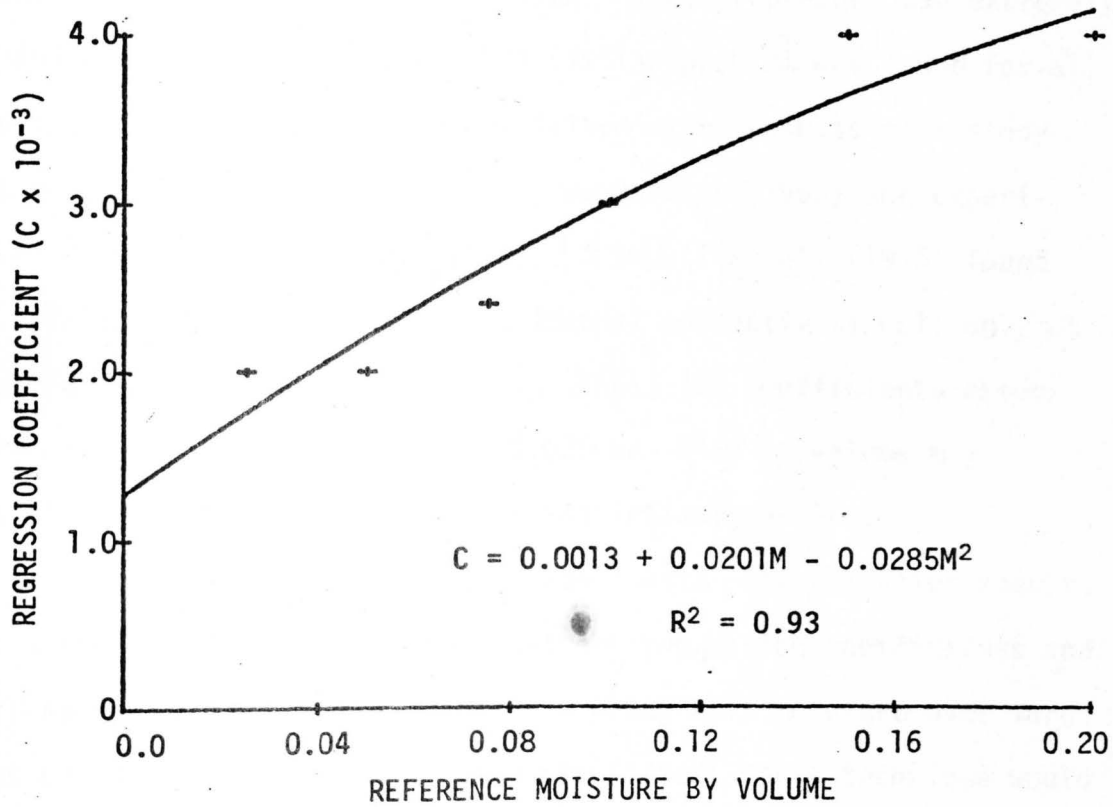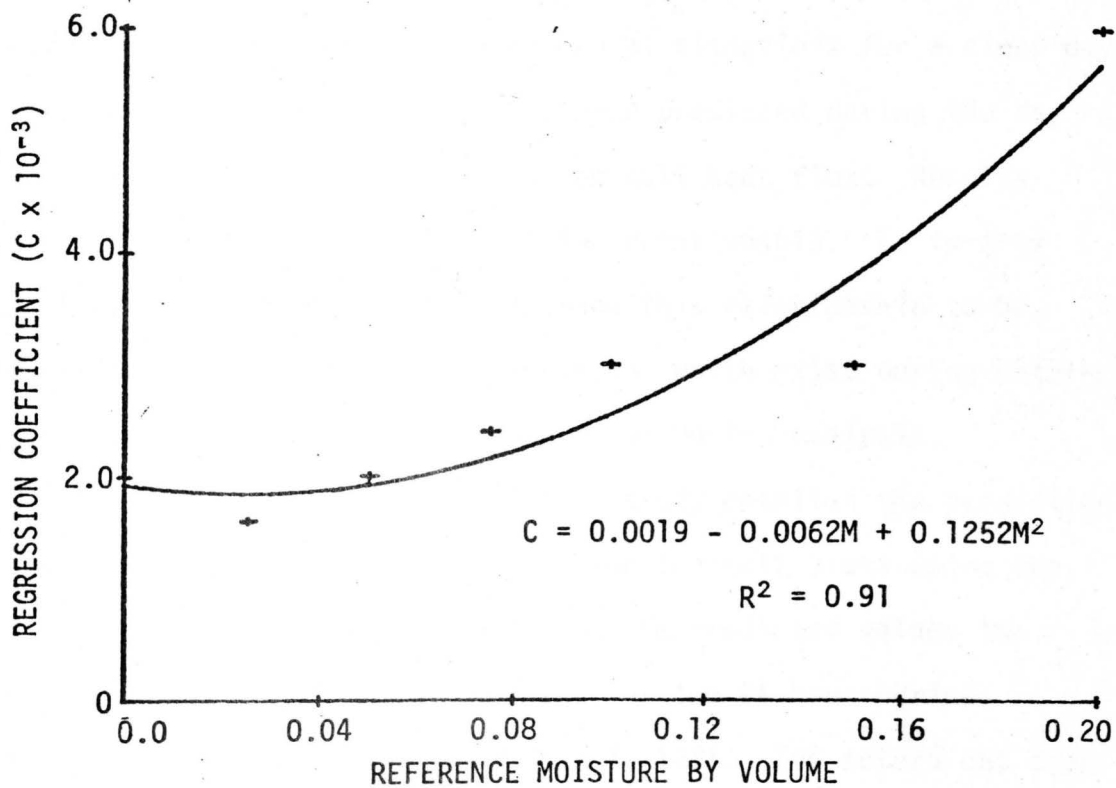
Figure 20. Reference plot soil moisture by volume as a function of the regression coefficient C for a 3 C° temperature difference at a depth of 50-cm.

Several calculations were also carried out to determine the dependence of the maximum surface temperature difference on soil heat flux. Values for soil heat flux and physical properties of the soil were again chosen to correpond to the experimental values previously used. Soil moisture by volume was assumed to be 10% in one plot and 20% in the second. Soil heat flux values were chosen to span a range which would include most experimental situations for a clear day. The maximum surface temperature difference predicted during the day was plotted as a function of the maximum soil heat flux. Results shown in Figure 21 display the resulting relationship. If further theoretical and experimental results show this relationship to be valid, differences in daily solar radiation which exist during satellite overpass could easily be accounted for during analysis.

The second major portion of this study entailed the prediction of surface temperature differences between two soil plots using the modified theoretical model and comparing the predicted values to experimental data. Data were collected for two 24 hour periods starting at 0100 hours, July 1 and July 7, 1981. Two mature oat crop covered soil plots were prepared as described above with one plot irrigated and the other left as a dryland plot. Values for porosity and bulk density are listed in Table 1 and are taken according to Beutler (1980). Other pertinent data were collected as previously described.

Apparent surface temperature was then plotted as a function of time for the July 1 dry-land plot and is shown in Figure 22. The
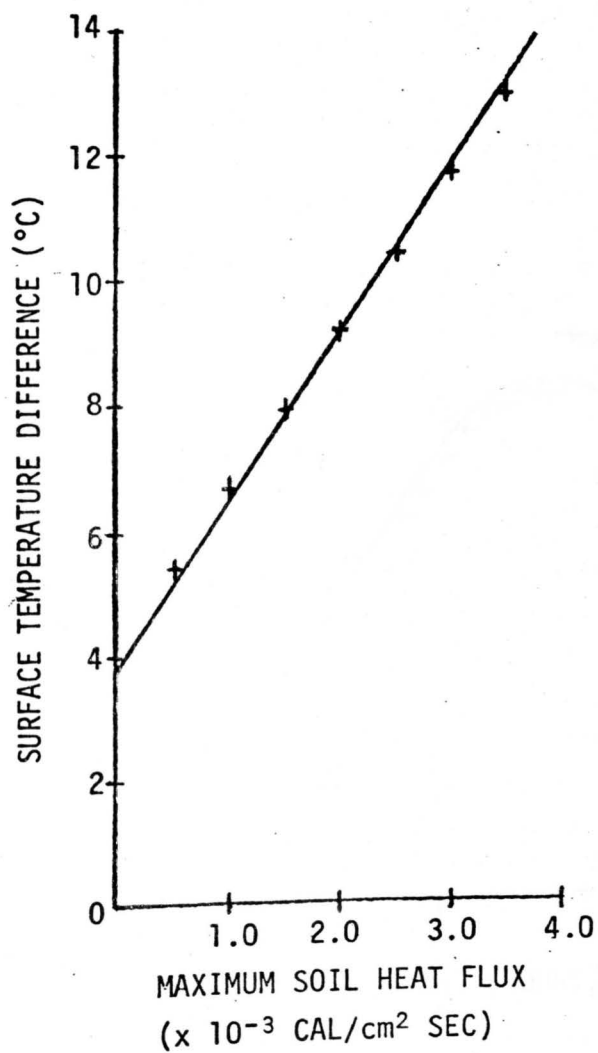
Figure 21. Calculated surface temperature difference between two plots as a function of soil heat flux amplitude. One plot is considered to have a constant soil moisture profile of 10% by volume while the other has a constant profile of 20%.
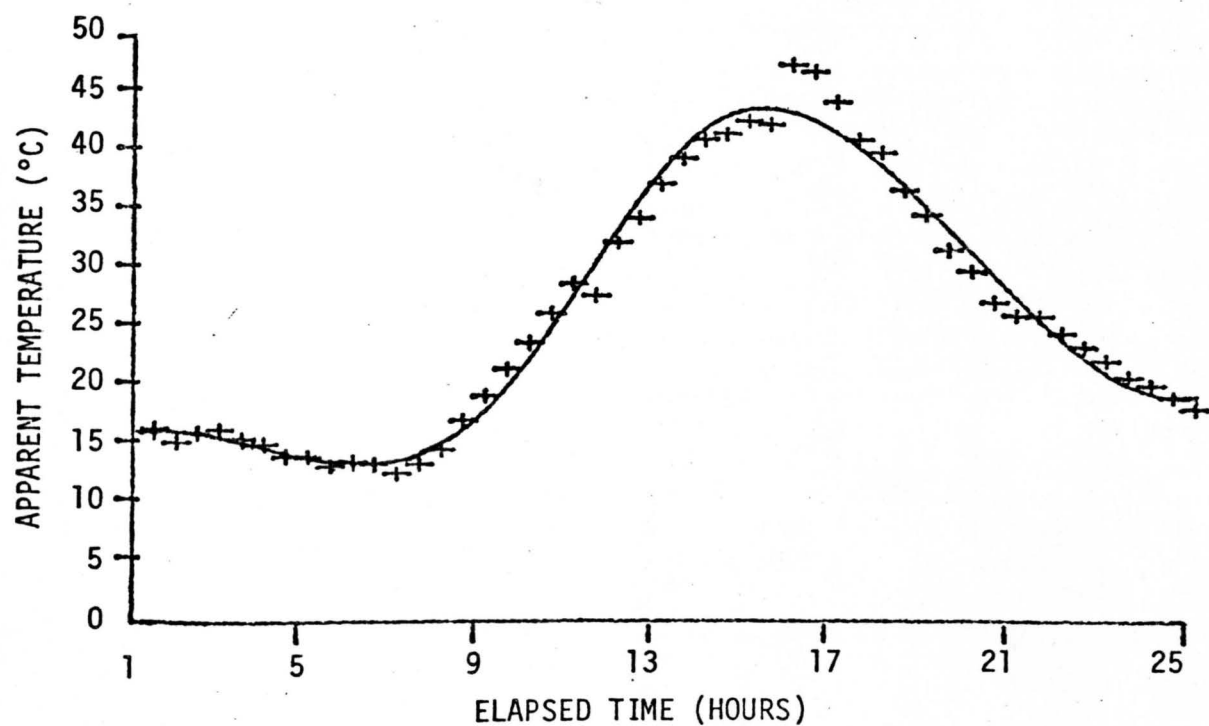
Figure 22. Apparent surface temperature over the oat crop cover
of the dry-land plot. Data collection begins at
0100 hours on July 1, 1981 and continues for 24
hours thereafter.

Table 1

Physical Properties of Soil Used

Depth (cm)	Porosity (E_a)	Bulk Density (g/cm^3)
1	.49	1.336
8	.47	1.379
25	.41	1.471
42	.39	1.579

Table 2

Soil Moisture Values Used

Depth (cm)	July 1		July 7	
	Wet (gm/cm^3)	Dry (gm/cm^3)	Wet (gm/cm^3)	Dry (gm/cm^3)
1	0.22	0.04	0.23	0.05
8	0.25	0.12	0.25	0.14
25	0.26	0.11	0.24	0.12
42	0.25	0.10	0.17	0.12

points are actual data points. The continuous curve was fit to the data using a cubic spline as described by Kimball (1976). The same data is shown in Figure 23 for the irrigated plot. Again a continuous curve was fit to the data using a cubic spline. The apparent surface temperature for the irrigated and dry-land plots are functionally similar. However, the apparent surface temperature variation for the irrigated plot during the diurnal cycle is smaller than dry-land temperature variation. This is consistent with previous results from studies by Beutler (1980) and Idso et al. (1975).

The apparent surface temperature difference for the diurnal cycle obtained by taking the difference of the cubic splines of Figures 22 and 23 is depicted in Figure 24. The functional form of the surface temperature difference is similar to the functional form of the surface temperature for the individual plots. This is also consistent with results by Beutler (1980). Note the surface temperature difference between the two plots approaches zero shortly after dawn. The maximum surface temperature difference is approximately 15.5 C° and occurs at roughly 1400 hours.

Surface temperature difference as a function of time for July 7 was obtained in precisely the same manner and is depicted in Figure 25. The maximum surface temperature difference for July 7 occurs at approximately 1400 hours and is approximately 7.5 C°. The reason for the smaller surface temperature differences for July 7 is the smaller moisture difference between the two plots during that time. Note that the surface temperature difference for July 7
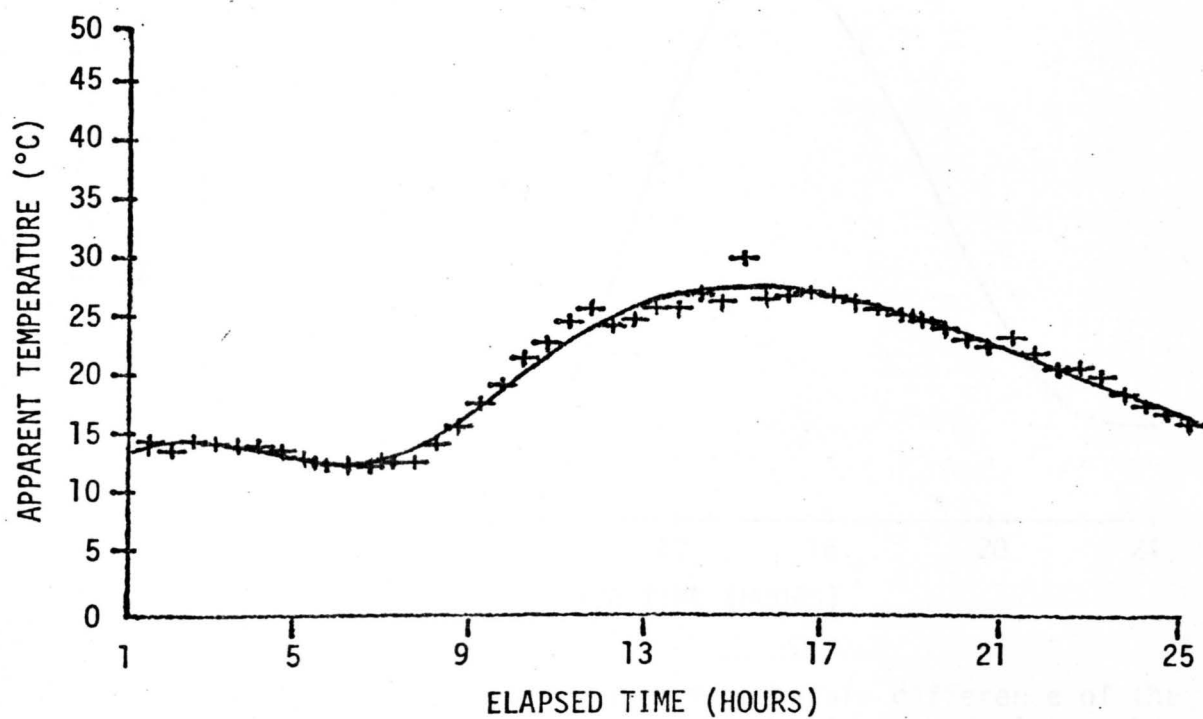
Figure 23. Apparent surface temperature over the oat crop cover of the irrigated plot. Data collection begins at 0100 hours on July 1, 1981 and continues for 24 hours thereafter.
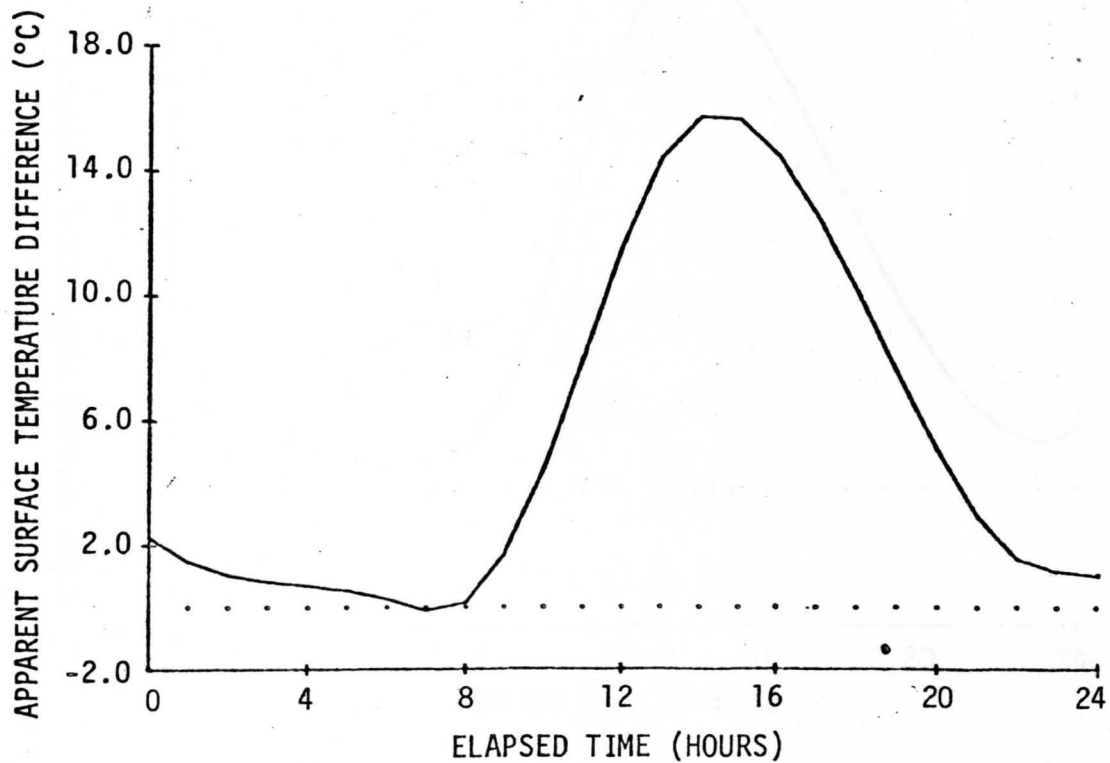
Figure 24. Apparent surface temperature difference of the dry-land and irrigated oat covered plots. Data is shown beginning at 0000 hours on July 1, 1981 and continuing for 24 hours thereafter.
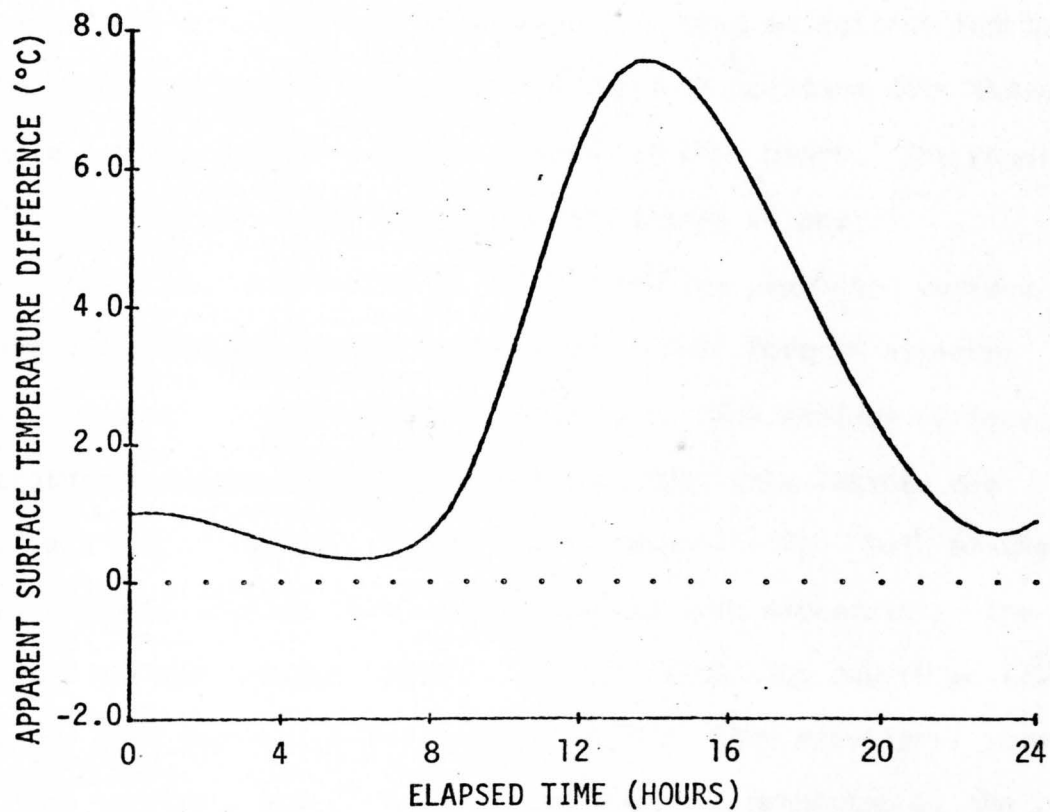
Figure 25. Apparent surface temperature difference of the dry-land and irrigated oat covered plots. Data is shown beginning at 0000 hours on July 7, 1981 and continuing for 24 hours thereafter.

approaches zero at approximately the same time as the previous data.

The original theoretical model by Beutler (1980) was then used as a function of time for both July 1 and July 7. The experimental values for the soil physical properties were used as initial inputs to the theoretical model together with the soil moisture data shown in Table 2 and actual temperature profile at 0100 hours. The results for July 1 and July 7 are illustrated in Figures 26 and 27.

Inspection of Figures 26 and 27 show the predicted surface temperature difference is of the same functional form as apparent surface temperature difference for both days. The maximum surface temperature differences obtained from the model calculations are 2.4 C° and 2.0 C° for July 1 and July 7, respectively. Both of these values are much smaller than values obtained from experiment. The predicted maximum surface temperature difference also occurs at 1200 hours for both days which is two hours earlier than experiment shows. Also, the temperature difference during night is predicted by the model to be approximately -1.2 C° for July 1 and -1.0 C° for July 7 which means the model predicts the surface temperature of the irrigated plot to be warmer than the dry-land plot which does not occur in experiment as previously shown. These results demonstrate the inadequacy of the model by Beutler (1980) to simulate the effects of a crop canopy.

The theoretical model was then modified to accept plant parameters and field structure parameters in addition to the already existing inputs to the theoretical model in an attempt to simulate

Figure 26. Theoretical model calculation of the surface
temperature difference between the dry-land and
irrigated oat covered plots for July 1, 1981.
The calculation is shown to begin at 0100 hours
and continues for 24 hours thereafter. The
effect of the crop cover is not considered.

Figure 27. Theoretical model calculation of the surface
temperature difference between the dry-land
and irrigated oat covered plots for July 7,
1981. The calculation is shown to begin at
0100 hours and continues for 24 hours there-
after. The effect of the crop cover is not
considered.

the shading effects of a crop canopy. The crop parameters were measured and estimated, but do not represent the results of a statis= tical study for obtaining the most representative values. The panicle of the individual oat plant was assumed to be the only source of shadowing on the soil surface. The dimensions of the assumed ellipsoidal shape of the panicle were 3.5 cm and 12.7 cm for the semiminor and semimajor axes respectively. The calculated value for plant density was 0.06 oat plants/cm^2. The distance between consecutive rows was 20.3 cm. Three leaf or grain kernel orientations were considered constant and at angles of $\pi/6$, $\pi/3$, and $\pi/2$ with respect to the soil surface at fractions of the canopy of 0.36, 0.27, and 0.17, respectively. The remaining fraction of the canopy was considered heliotropic and thus maintained a constant angle of $\pi/2$ with respect to the solar altitude. These values for the various parameters were used in theoretical model calculations for both July 1 and July 7. In addition, the insulating effect of the canopy was also included in the theoretical model modifications. This result adds the effective canopy temperature of both the dry-land and irrigated plots and the fraction of sky directly above any point on the soil surface obstructed by the canopy as inputs to the model.

The surface heat flux with the light penetration model during the daylight hours is plotted as a function of time in Figure 28. Also shown is the surface heat flux as calculated for a bare soil surface. The light penetration model lowers the maximum value for soil heat flux by 40% and also slightly changes the functional form. The maximum surface heat flux for the bare soil occurs at 1230 hours
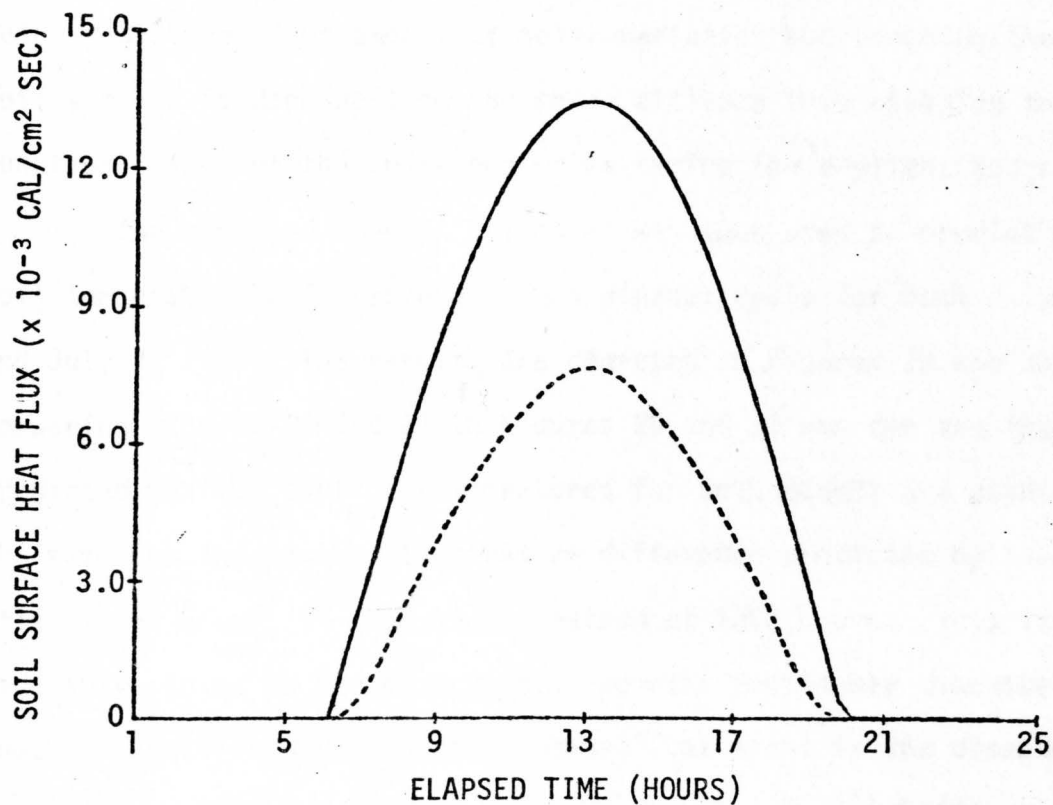
Figure 28. Comparison of the calculated soil surface heat flux, during the day, not considering the shadowing effect of the crop danopy, with soil surface heat flux including the effect of the crop canopy.

Heat Flux Original Model ——————

Heat Flux Modified Model ----------

compared to 1300 hours for the plant canopy situation. The later occurring maximum heat flux is probably due to the different orientations of parts of the plant canopy. The smaller heat flux is due to the fact that the crop canopy intercepts a portion of the incoming solar radiation. The amount of solar radiation not reaching the soil surface is dependent on the solar altitude thus changing the functional form of the solar heat flux during the daylight hours.

The modified theoretical model was then used to predict the soil temperature difference during a diurnal cycle for both July 1 and July 7, 1981. The results are depicted in Figures 29 and 30. Comparing Figures 26 and 27 to Figures 29 and 30 one can see that the predicted maximum surface temperatures for both models are essentially the same but the maximum temperature difference predicted by the modified model occurs at 1300 hours instead of 1200 hours. This is considerably closer to the experimental results previously discussed. Another result from the modified theoretical model is the disappearance of a surface temperature difference during the nighttime hours as was observed experimentally.

The predicted surface temperature difference for both July 1 and July 7 are of the same functional form as the experimental apparent surface temperature differences depicted in Figures 24 and 25. These results indicate that the modifications to the theoretical model contribute substantially to the accuracy of predicting surface temperature difference during the nighttime hours. However, the model may require further modification to better predict the magnitudes of daylight surface temperature differences.
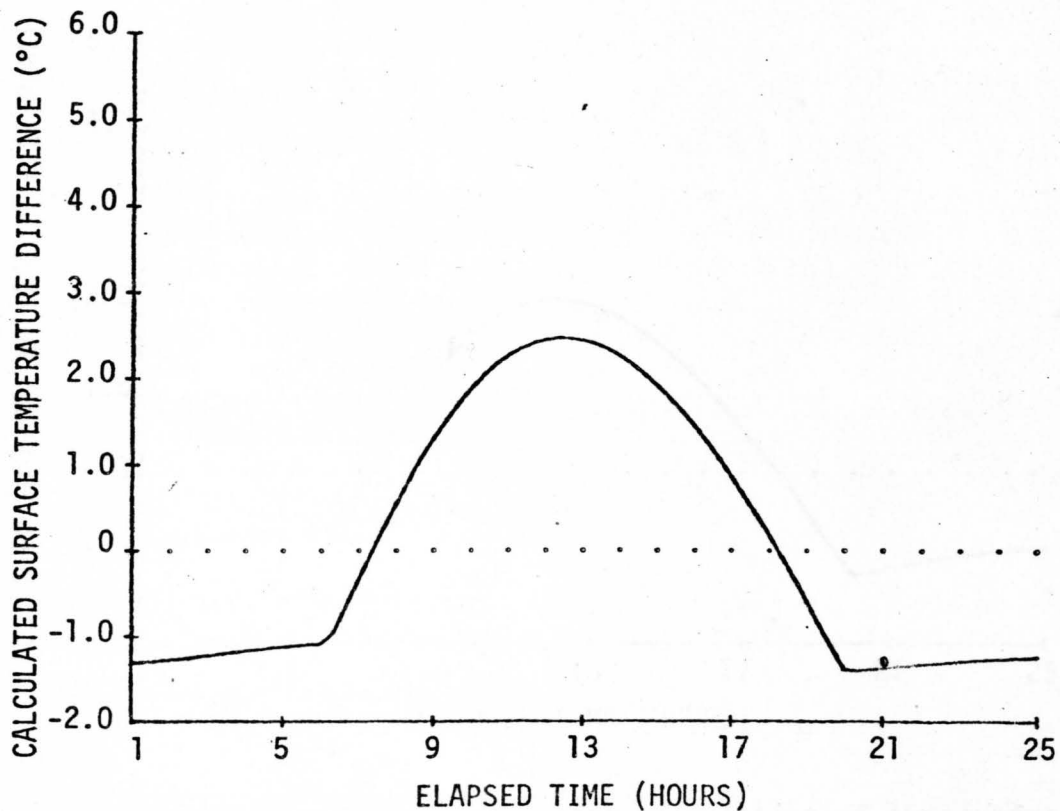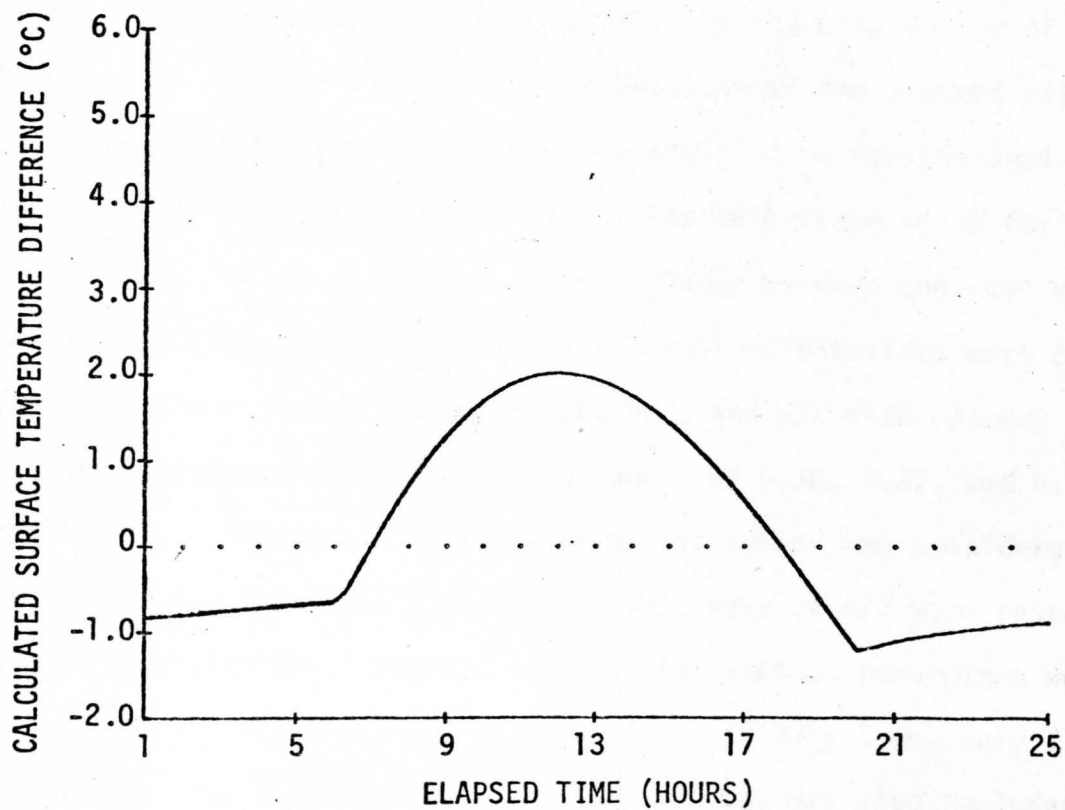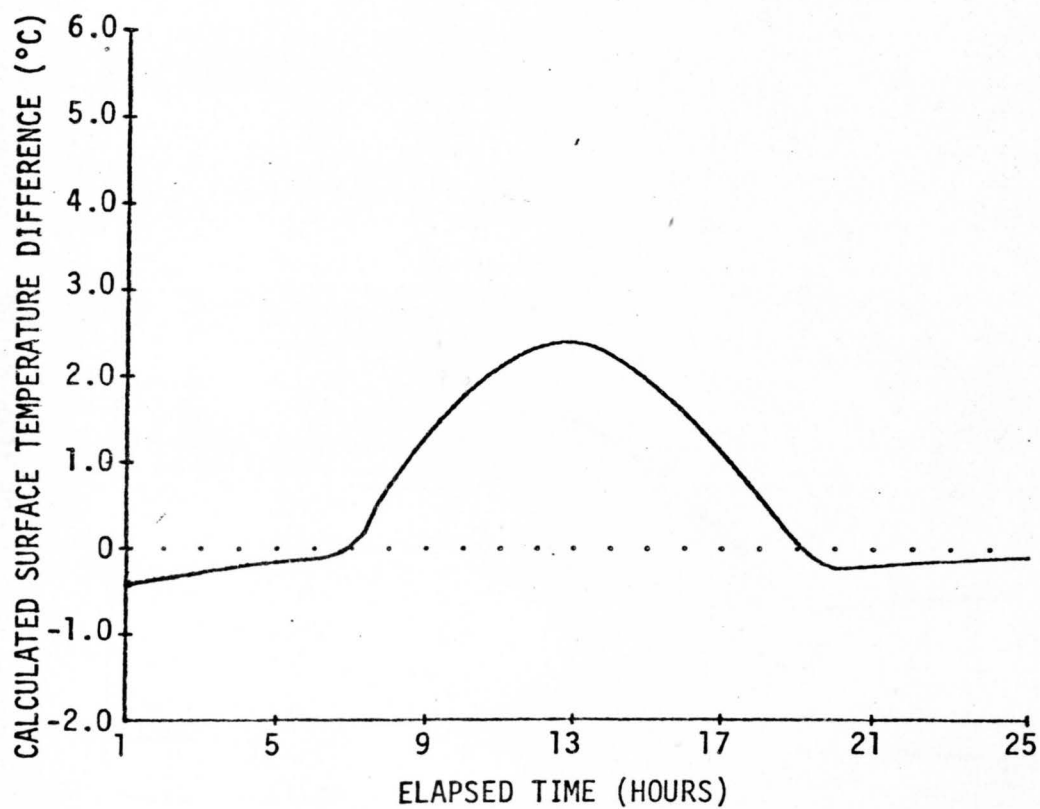
Figure 29. Theoretical model calculation of the surface
temperature difference between the dry-land
and irrigated oat crop covered plots for July 1,
1981. The calculation is shown to begin at
0100 hours and continues for a 24 hour period.
The effect of the crop canopy is included in
the calculation.
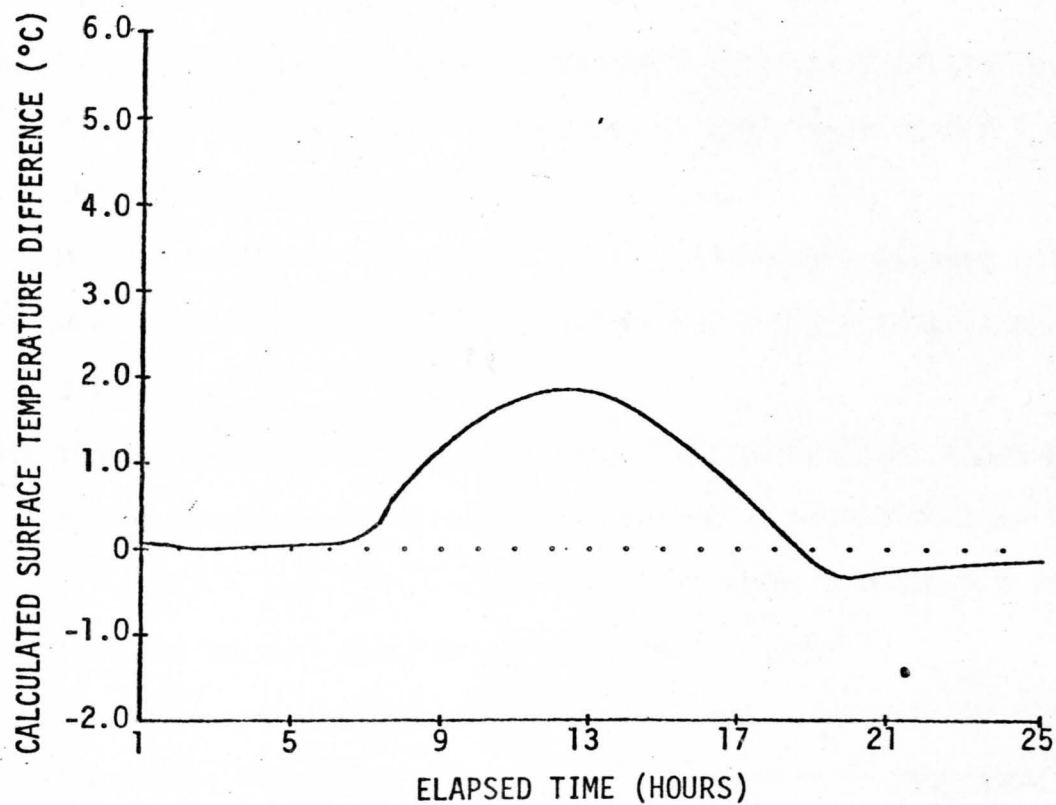
Figure 30. Theoretical model calculation of the surface
temperature difference between the dry-land
and irrigated oat covered plots for July 7,
1981. The calculation is shown to begin at
0100 hours and continues for a 24 hour period.
The effect of the crop cover is included in
the calculation.

CONCLUSIONS

1. Model calculations predict a well defined quadratic relationship between maximum surface temperature difference and soil moisture difference.

2. Statistical analysis shows a quadratic dependence of the coefficients for the quadratic equation of conclusion number 1 on the reference plot moisture.

3. Model calculations predict a linear relationship between soil heat flux at the surface and the maximum surface temperature difference.

4. The surface temperature differences for the daylight hours predicted by the modified model are smaller in magnitude than the experimental apparent surface temperature differences but have the same general functional dependence on time.

5. The predicted surface temperature differences during the nighttime hours using the modified model is similar in magnitude to the experimental nighttime apparent surface temperature differences.

6. The results of this study in general show great promise for the use of satellite thermal emittance data in determining soil moisture over large areas of the earth using the following method. A group of sites is chosen over the area considered with at least one site chosen as a reference site where soil moisture will be ground-truth monitored. Using the reference soil moisture, the coefficients of the quadratic equation relating soil moisture

difference to maximum surface temperature difference can be obtained. Using the apparent surface temperature differences obtained from satellite TIR and corrected for variation in solar radiation the soil moisture differences between the reference site and the other sites can be determined. Since the reference site moisture would be known the soil moisture can be easily determined for the other sites.

SUGGESTIONS FOR FURTHER STUDY

The quadratic relationship found to exist between soil moisture difference and calculated maximum surface temperature difference needs to be further confirmed by experiment. The data collection would require the monitoring of soil moisture in both soil plots and the capability to change content of either plot independently of the other. The same experimental method as used in this study is appropriate but data must be collected for much greater variation of reference soil moistures.

The quadratic relationship between the regression coefficients obtained from the relationship between soil moisture difference and calculated maximum surface temperature difference could be investigated further. Kimball et al. (1975) found that the method by DeVries (1963) for calculating thermal conductivity agreed well with experimental data only at intermediate soil moisture contents. Thus, the functional relationship between the reference site moisture and the regression coefficients and constants may be further defined and understood if intermediate reference soil moistures, between 5% and 18% by volume, are used in all further theoretical model calculations.

The theoretical model in its present form does not predict the magnitude of maximum daylight surface temperature difference with a great deal of accuracy. There are two possible methods by which the theoretical model may be refined and modified to simulate surface temperature difference between two points on the earth with greater accuracy. The first method would require a statistical study of

crop parameters to determine the most representative values of plant density, the lengths of the semimajor and semiminor axes, and etc.

The second method would require modification of the model to simulate the energy lost from the surface due to evaporation from the soil and evapotranspiration from the plant canopy. This model would require air temperature, humidity, wind velocity, and remotely sensed surface temperature data for the calculation of the energy budget at the soil surface when the energy lost to evaporation is simulated (Idso et al., 1975; Idso et al., 1977). When a crop canopy is present the model would also require a remotely sensed effective crop canopy temperature to predict the energy lost due to the evapotranspiration from the crop canopy (Kanemasu et al., 1976).

LITERATURE CITED

Aaron, D.B., J.A. Tunheim and D.G. Moore, 1976, "Soil Temperature Fields Associated with Saline Seeps," Proceedings of South Dakota Academy of Science, Vol. 55, pp. 25-36.

Beutler, G.A., 1980, Model Development for Predicting Soil Moisture By Thermography, South Dakota State University, M.S. Thesis, 77 pp.

Blad, B.L. and N.J. Rosenberg, 1976, "Measurement of Crop Temperature by Leaf Thermocouple, Infrared Thermometry and Remotely Sensed Thermal Imagery," Agronomy Journal, 68:635-641.

Carson, J.E., 1961, "Soil Temperature and Weather Conditions," AEC Research and Development Report ANL-64-70, Argonne, Illinois, p. 244.

Cartwright, K., 1968, "Thermal Prospecting for Groundwater," Water Resources Res., 4:395-401.

DeVries, D.A., in Physics of Plant Environment, Van Wijk, W.R., Ed., North-Holland Publishing Company, Amsterdam, 1963.

Fleagle, R.G., 1950, "Radiation Theory of Local Temperature Differences," Journal of Meteorology, 7:114-119.

Gillespie, A.R. and A.B. Kahle, 1977, "Constructive and Interpretation of a Digital Thermal Inertia Image," Photogrammetric Engineering and Remote Sensing, 43:983-1000.

Heilman, J.L. and D.G. Moore, 1981, "HCMM Detection of High Soil Moisture Areas," Final Report for Goddard Space Flight Center, Contract NAS 5-24206, Greenbelt, Maryland, pp. 34-59.

Heilman, J.L. and D.G. Moore, 1980, "Thermography for Estimating Near-Surface Soil Moisture under Developing Crop Canopies," Journal of Applied Meteorology, 19:324-328.

Idso, S.B., R.D. Jackson and R.J. Reginato, 1975, "Estimating Evaporation: A Technique Adaptable to Remote Sensing," Science, 189, 991-992.

Idso, S.B., R.J. Reginato and R.D. Jackson, 1977, "An Equation for Potential Evaporation from Soil, Water, and Crop Surfaces Adaptable to use by Remote Sensing," Geophysical Research Letters, Vol. 4, pp. 187-188.

Idso, S.B., T.J. Schmugge, R.D. Jackson and R.J. Reginato, 1975, "The Utility of Surface Temperature Measurements for Remote Sensing of Surface Soil Status," Journal of Geophysical Research, 80:3044-3049.

Kahle, A.B., A.R. Gillespie, A.F.H. Goetz and J.D. Addington, 1975, "Thermal Inertia Mapping," Proceedings, 10th International Symposium on Remote Sensing of the Environment, Ann Arbor, Michigan, pp. 985-994.

Kanemasu, E.T., L.R. Stone and W.L. Powers, 1976, "Evapotranspiration Model Tested for Soybean and Sorghum," Agronomy Journal, 68:569-572.

Kimball, B.A., 1976, "Smoothing Data with Cubic Splines," Agronomy Journal, 68:126-129.

Kimball, B.A., R.D. Jackson, R.J. Reginato, F.S. Nakayama and S.B. Idso, 1976, "Comparison of Field-measured and Calculated Soil-heat Fluxes," Soil Science Society of America Journal, 40:18-28.

Mann, J.E., G.L. Curry, D.W. DeMichele and D.N. Baker, 1980, "Light Penetration in a Row-Crop with Random Plant Spacing," Agronomy Journal, 72:131-139.

Meyer, C.R., 1972, Simulation of a Surface Thermal Anomaly, South Dakota State University, M.S. Thesis (Unpublished).

Moore, D.G., M.L. Horton, M.J. Russel and V.I. Myers, 1975, "Evaluation of Thermal X/5 Detector Skylab S-192 Data for Estimating Evaporation and Thermal Properties of Soils for Irrigation Management," Proceedings of the NASA Earth Resources Survey Symposium, Houston, Texas, NASA TM-X58168:2561-2583.

Moore, D.G. and V.I. Myers, 1972, "Environmental Factors Affecting Thermal Groundwater Mapping." Report No. RSI 72-06, presented to U.S.G.S., Department of the Interior, 23 pp.

Myers, V.I. and M.D. Heilman, 1969, Thermal Infrared for Soil Temperature Studies Photogrametric Engineering, 35:1024-1032.

Myers, V.I. and D.G. Moore, 1972, "Remote Sensing for Defining Aquifers in Glatial Drift," Proceedings of the Eighth International Symposium of Remote Sensing of Environment, Ann Arbor, Michigan, 2-6, October 1972, pp. 715-728.

Reginato, R.J., S.B. Idso, J.F. Vedder, R.D. Jackson, M.B. Blanchard
and R. Goettelman, 1976, "Soil Water Content and Evaporation
Determined by Thermal Parameters Obtained from Ground-Based
and Remote Measurements," Journal Geophysics Research,
81:1617-1620.

Schmugge, T., 1978, "Remote Sensing of Surface Soil Moisture,"
Journal of Applied Meterorology, 17:1549-1557.

Schmugge, T.J., P. Gloersen, T. Wilheit and F. Geiger, 1974, "Remote
Sensing of Soil Moisture with Microwave Radiometers,"
Journal of Geophysics Research, 79:317-323.

Smith, R.W., 1969, "Thermal Dynamics at the Earth-Air Interface: The
Implications for Remote Sensing of the Geological Environ-
ment," Report No. RSL 69-4, Stanford, California.

Tunheim, J.A., 1977, "Application of Heat-Flow Temperature Model for
Remotely Assessing Near Surface Soil Moisture by Thermography,"
OWRT Completion Report, Project A-053-SDAK, Agreement
No. 14-31-0001-6043.

Wilson, W.J., 1967, "Stand Structure and Light Penetration: III
Sunlit Foliage Area," Journal of Applied Ecology, 4:159-165.

APPENDIX

HPL PROGRAM FOR FINITE-DIFFERENCE HEAT FLOW SIMULATION MODEL

The following program listing is written in a language used by Hewlett-Packard in the 9835A mini-computer furnished by the Water Resources Institute at South Dakota State University

A[*]	Temperature of Profile A
B[*]	Temperature of Profile B
C[*]	Conductivity of Profile A
D[0]-D[50]	Conductivity of Profile B
D[51]	Fraction of field covered by the canopy oriented at angle α_1
D[52]	Fraction of field covered by the canopy oriented at angle α_2
D[53]	Fraction of field covered by the canopy oriented at angle α_3
E[0]-E[50]	Heat Capacity of Profile A
E[I]	Term used by Mann in calculation of the fraction of a single plant canopy projection which lies in strip type A
F[0]-F[50]	Heat Capacity of Profile B
F[51]	Angle α_1
F[52]	Angle α_2
F[53]	Angle α_3
H[*]	Time of day (hour)
G[0]	Term used by DeVries in calculation of conductivity
G[1]	Heat capacity of water
G[2]	Heat capacity of soil

H[1]	Initial starting hour
H[2]	Ending hour
K[0]	Conductivity of air
K[1]	Conductivity of water
K[2]	Conductivity of soil
M[1]	Initial starting minute
M[2]	Minute when calculation is to end
O[*]	Soil moisture for site A
P[*]	Soil moisture for site B
R[0]-R[50]	Allocation to store old temperature for site A
R[51]	Semiminor axis length of individual ellipsoidal plant canopy
R[52]	Semimajor axis length of individual ellipsoidal plant canopy
R[53]	Angle between the solar azimuth and the direction parallel to the rows of the crop
R[54]	Maximum number of rows shielding any point in strip type B
R[55]	Plant density
R[56]	Angle between heliotropic part of plant canopy and solar altitude assumed to be $\pi/2$
R[57]	Distance between consecutive crop rows
R[58]	Fraction of the plant canopy that is heliotropic
R[59]	Fraction of the field shielded by canopy projection on to the field
S[*]	Allocation to store old temperature for site B
U[0:50]	Aeration porosity for site A
V[0;50]	Aeration porosity for site B

W[1]	Effective air temperature
W[2]	Amount of soil by volume at 1-cm depth
W[3]	Amount of soil by volume at 8-cm depth
W[4]	Amount of soil by volume at 24-cm depth
W[5]	Amount of soil by volume at 42-cm depth
X[1]	Distance between nodal points
Y[1]	Ending day
A	Soil heat flux for site A
B	Soil heat flux for site B
C	Time from sunrise to solar noon
D,E,F,G	Soil bulk density at 1, 8, 24, and 42 centimeters
I	Counter
J	Counter
K	Counter
L	Length of day
M	Amplitude of soil heat flux for site A
N	Number of equally spaced nodal points
P	Time between printouts
Q	Amplitude of soil heat flux for site B
R	Dummy variable
T	Time interval between calculation in seconds
X	Dummy variable
r29	Fractional area of the field which lies in strip type A
r31	Area of individual plant canopy projection onto the field

r^{32} Total area of all plant canopy projections
which fall into strips of type A per unit
field area

r^{33} Total area of all plant canopy projections
which fall into strips of type B per unit
field area

r^{37} Fraction of entire field in direct sunlight

r^{57} Fraction of a single plant canopy projection
which lies in strip type A

r^{73} Ratio of the obstructed area to the total area
of a hemisphere circumscribed above the
radiating point on the soil surface

r^{74} Dry-land site canopy effective temperature

r^{75} Irrigated site canopy effective temperature

r^{76} Dummy variable

PROGRAM LISTING (HPL)

Operational Procedure

```
0: 706→r0;gto 74
```

Subroutine for Soil Heat Flux

```
1: "QHEAT":M[1]/60→r21
2: H[1]+r21→r22
3: r22-C→r23
4: (W[1]+273.16)/100→r24;r76*(r74+273.16)/100→r77
5: (A[0]+273.16)/100→r25;r76*(r75+273.16)/100→r78
6: (B[0]+273.16)/100→r26
7: .000136*r24↑4→r60;(1-r73)*.65*r80→r80
8: -(.000136*(r25↑4-r73*r77↑4)-r80)→r11
9: -(.000136*(r26↑4-r73*r78↑4)-r80)→r12
10: if r23<=0;gto 61
11: if r23>=L;gto 61
12: rad
13: if r39=0;M*sin(r23*π/L)+r11→r11
14: if r41=0;Q*sin(r23*π/L)+r12→r12
15: if r39=0 and r41=0;gto 61
16: (cos(π*r23/L)/sin(π*r23/L))↑2→r27
17: (R[51]↑2+R[52]↑2*r27)↑(1/2)→r27
18: (cos(π*r23/L)/sin(π*r23/L))↑2*sin(R[53])↑2→r28
19: 1+(R[52]/R[51])↑2*r28→r28
20: 2*R[52]*r28↑(1/2)/R[57]→r28
21: if 0<r28 and r26<=1;1→R[54]
22: if 1<r28 and r28<=2;2→R[54]
23: if 2<r28 and r28<=3;3→R[54]
24: if 3<r28 and r28<=4;4→R[54]
25: if 4<r28 and r28<=5;5→R[54]
26: if 5<r28 and r28<=6;6→R[54]
27: if 6<r28 and r28<=7;7→R[54]
28: if 7<r28 and r28<=8;8→R[54]
29: if 8<r28 and r28<=9;9→R[54]
30: if 9<r28 and r28<=10;10→R[54]
31: if r23>6 and r28>10;r37-.0035→r37;gto 59
32: if r23<6 and r28>10;.0038+r37→r37;gto 59
33: R[54]-r28→r29;0→r57
34: if R[54]=1;gto 40
35: for I=51 to 49+R[54]
36: (2(I-50)-r28)/r28→E[I]
37: asn(E[I])+E[I]*(1-E[I]↑2)↑(1/2)→E[I]
38: E[I]*2/π→r30;r30+r57→r57
39: next I
40: r27*R[51]*π→r31
41: if r29=0;R[55]*r31*r57→r32;gto 43
42: R[55]*r31*r57/r29→r32
43: R[55]*r31*(1-r57)/(1-r29)→r33
44: for I=51 to 53
45: if 0<=F[I] and F[I]<=π*r23/L;gto 48
46: if π*r23/L<F[I] and F[I]< π/2;gto 49
47: if F[I]=π/2;gto 52
48: D[I]*cos(F[I])→P[I];gto 53
49: asc (tan(π*r23/L)*cos(F[I])/sin(F[I]))→r34
50: 1+2*((tan(r34)-r34)/π)→P[I]
```

Subroutine for Soil Heat Flux Continued

```
51: D[I]*cos(F[I])*P[I]+P[I];gto 53
52: D[I]*(2/π)*cos(π*r23/L)/sin(π*r23/L)+P[I]
53: next I
54: R[51]+R[52]+R[53]+R[59]
55: R[58]*(sin(R[56])/sin(π*r23/L))+R[59]+R[59]
56: R[59]/(R[55]*r31)+r35
57: 1-exp(-r35)+r36
58: r29*exp(-r32*r36)+(1-r29)*exp(-r33*r36)+.1+r37
59: if r39=1;r37*M+r70;r70*sin(r23*π/L)+r11+r11
60: if r41=1;Q*r37+r70;r70*sin(r23*π/L)+r12+r12
61: r11+A;r12+B;ret
```

Subroutine for Conductivities in Profile A

```
62: "CONDUC A":
63: .333-O[I]/(1-W[X])*(.333-.035)+G[0]
64: .0000615+.00196*O[I]+K[0]
65: (2/(1+(K[2]/K[1]-1)*G[0])+1/(1+(K[2]/K[1]-1)*(1-2*G[0])))/3+r1
66: (2/(1+(K[0]/K[1]-1)*G[0])+1/(1+(K[0]/K[1]-1)*(1-2*G[0])))/3+r2
67: ret
```

Subroutine for Conductivities in Profile B

```
68: "CONDUC B":
69: .333-V[I]/(1-W[X])*(.333-.035)+G[0]
70: .0000615+.00196*P[I]+K[0]
71: (2/(1+(K[3]/K[1]-1)*G[0])+1/(1+(K[3]/K[1]-1)*(1-2*G[0])))/3+r3
72: (2/(1+(K[0]/K[1]-1)*G[0])+1/(1+(K[0]/K[1]-1)*(1-2*G[0])))/3+r2
73: ret
```

Dimension Statements

```
74: dim A[0:50],B[0:50],C[0:50],D[0:53],E[0:60],F[0:53],O[0:230],P[0:53]
75: dim X[1],V[0:230],W[5],E$[4]
76: dim M[0:4],H[0:2],K[0:3],G[0:2],Y[0:1],R[0:59],S[0:51],U[0:230]
```

Program Parameter Assignments

```
77: 1+Y[1];60+T;50+N;0+M[1];1+H[1];0+M[2];1+H[2];1+X[1]
```

Entering of Calculation Parameters

```
78: ent P,R[51],R[52],R[53],R[55],R[56],R[57],R[58]
79: ent F[51],F[52],F[53],D[51],D[52],D[53],W[1],r73,r74,r75
80: ent "CROP COVER A ? YES=1,NO=0",r38
81: if r38=1;1→r39
82: if r38=0;0→r39
83: ent "CROP COVER B? YES=1,NO=0",r40
84: if r40=1;1→r41
85: if r40=0;0→r41
```

Procedural Step

```
86: 0→J→M[3]→M[4]→r10
87: H[1]*60+M[1]→M[3]
88: 1→r13
```

Entering of Soil Temperature Profiles

```
89: ent A[0],A[1],A[5],A[10],A[25],A[50],B[0],B[1],B[5],B[10],B[25],B[50]
```

Interpolation of Soil Temperatures

```
90: for I=2 to 4;(A[5]-A[1])/4*(I-1)+A[1]→A[I]
91: (B[5]-B[1])/4*(I-1)+B[1]→B[I];next I
92: for I=6 to 9;(A[10]-A[5])/5*(I-5)+A[5]→A[1]
93: (B[10]-B[5])/5*(I-5)+B[5]→B[I];next I
94: for I=11 to 24;(A[25]-A[10])/15*(I-10)+A[10]→A[I]
95: (B[25]-B[10])/15*(I-10)+B[10]→B[I];next I
96: for I=26 to 49;(A[50]-A[25])/25*(I-25)+A[25]→A[I]
97: (B[50]-B[25])/25*(I-25)+B[25]→B[I];next I
```

Surface Temperature Difference

```
98: A[0]-B[0]→S[51]
```

Determination of Mode for Entering Heat Capacity and Thermal Conductivity

99: J+1→J;if J>1;gto 146

Entering of Soil Physical Parameters

100: ent O[1],O[8],O[25],O[42],P[1],P[8],P[25],P[42],W[2],W[3],W[4],W[5]
101: ent K[1],K[2],K[3],G[1],G[2],D,E,F,G,M,Q,C,L,r76

Calculation of Percent Moisture by Volume

102: O[1]*D→O[1];O[8]*E→O[8];O[25]*F→O[25];O[42]*G→O[42]
103: P[1]*D→P[1];P[8]*E→P[8];P[25]*F→P[25];P[42]*G→P[42]

Calculation of Percent Air

104: 1-O[1]-W[2]→U[1]
105: 1-P[1]-W[2]→V[1]
106: 1-O[8]-W[3]→U[8]
107: 1-P[8]-W[3]→V[8]
108: 1-O[25]-W[4]→U[25]
109: 1-P[25]-W[4]→V[25]
110: 1-O[42]-W[5]→U[42]
111: 1-P[42]-W[5]→V[42]

Specification of Thermal Conductivities

112: 1→I;2→X;cll 'CONDUC A'(U[I],O[I],W[X])
113: (O[1]*K[1]+r1*W[2]*K[2]+r2*U[1]*K[0])/(O[1]+r1*W[2]+r2*U[1])→C[1]
114: 1→I;2→X;cll 'CONDUC B'(V[I],P[I],W[X])
115: (P[1]*K[1]+r3*W[2]*K[3]+r2*V[1]*K[0])/(P[1]+r3*W[2]+r2*V[1])→D[1]
116: 8→I;3→X;cll 'CONDUC A'(U[I],O[I],W[X])
117: (O[8]*K[1]+r1*W[3]*K[2]+r2*U[8]*K[0])/(O[8]+r1*W[3]+r2*U[8])→C[8]
118: 8→I;3→X;cll 'CONDUC B'(V[I],P[I],W[X])
119: (P[8]*K[1]+r3*W[3]*K[3]+r2*V[8]*K[0])/(P[8]+r3*W[3]+r2*V[8])→D[8]
120: 25→I;4→X;cll 'CONDUC A'(U[I],O[I],W[X])
121: (O[25]*K[1]+r1*W[4]*K[2]+r2*U[25]*K[0])/(O[25]+r1*W[4]+r2*U[25])→C[25]
122: 25→I;4→X;cll 'CONDUC B'(V[I],P[I],W[X])
123: (P[25]*K[1]+r3*W[4]*K[3]+r2*V[25]*K[0])/(P[25]+r3*W[4]+r2*V[25])→D[25]
124: 42→I;5→X;cll 'CONDUC A'(U[I],O[I]W[X])
125: (O[42]*K[1]+r1*W[5]*K[2]+r2*U[42]*K[0])/(O[42]+r1*W[5]+r2*U[42])→C[42]
126: 42→I;5→X;cll 'CONDUC B'(V[I],P[I],W[X])
127: (P[42]*K[1]+r3*W[5]*K[3]+r2*V[42]*K[0])/(P[42]+r3*W[5]+r2*V[42])→D[42]

82

Specification of Heat Capacity

```
128: W[2]*G[2]+O[1]*G[1]→E[1]
129: W[2]*G[2]+P[1]*G[1]→F[1]
130: W[3]*G[2]+O[8]*G[1]→E[8]
131: W[3]*G[2]+P[8]*G[1]→F[8]
132: W[4]*G[2]+O[25]*G[1]→E[25]
133: W[4]*G[2]+P[25]*G[1]→F[25]
134: W[5]*G[2]+O[42]*G[1]→E[42]
135: W[5]*G[2]+P[42]*G[1]→F[42]
```

Interpolation of Thermal Conductivities and Heat Capacity

```
136: for I=2 to 24;C[8]-(C[25]-C[8])/17*(8-I)→C[I]
137: D[8]-(D[25]-D[8])/17*(8-I)→D[I]
138: E[8]-(E[25]-E[8])/17*(8-I)→E[I]
139: F[8]-(F[25]-F[8])/17*(8-I)→F[I];next I
140: for I=26 to 50;C[25]+(C[42]-C[25])/17*(I-25)→C[I]
141: D[25]+(D[42]-D[25])/17*(I-25)→D[I]
142: E[25]+(E[42]-E[25])/17*(I-25)→E[I]
143: F[25]+(F[42]-F[25])/17*(I-25)→F[I];next I
144: C[1]→C[0];D[1]→D[0];E[1]→E[0];F[1]→F[0]
```

Time Interval Between Calculations

```
145: T/(2*X[1]*X[1])→r1;gto 160
```

Call for Soil Heat Flux Subroutine

```
146: cll 'QHEAT'
```

Calculation of Nodal Temperatures and Lower Boundry

```
147: for I=1 to N-1;(E[I]/r1-C[I-1]-2*C[I]-C[I+1])*A[I]→r6
148: ((C[I-1]+C[I])*A[I-1]+(C[I]+C[I+1])*A[I+1]+r6)*r1/E[I]→R[I]
149: (F[I]/r1-D[I-1]-2*D[I]-D[I+1])*B[I]→r7
150: ((D[I-1]+D[I])*B[I-1]+(D[I]+D[I+1])*B[I+1]+r7)*r1/F[I]→S[I];next I
151: 4*X[1]*r11+(E[1]/r1-2*C[1]-2*C[2])*A[0]+(2*C[1]+2*C[2])*A[1]→R[0]
152: r1/E[1]*R[0]→R[0]
153: 4*X[1]*r12+(F[1]/r1-2*D[1]-2*D[2])*B[0]+(2*D[1]+2*D[2])*B[1]→S[0]
154: r1/F[1]*S[0]→S[0]
155: A[N]→R[N]
156: B[N]→S[N]
```

Reassignment of Nodal Temperature for Succeeding Iteration

```
157: for I=0 to N;R[I]→A[I];S[I]→B[I];next I
158: A[0]-B[0]→S[51]
```

Test for Printout Time

```
159: if M[4]<P;gto 183
```

Printout of Pertinent Data

```
160: r10+1→r10
161: int(r10/2)→r11;r11*2→r12
162: fmt 1,4/,"TEMPERATURE PROFILE AT  ",fz2.0,fz2.0," HOURS"
163: wrt 706.1,H[1],M[1]
164: fmt 2,/,/,"SURFACE TEMPERATURE DIFFERENCE =",f6.3
165: wrt 706.2,S[51]
166: fmt 4,/,"SOIL HEAT FLUX SITE A = ",f12.9,"  SITE B = ",f12.9
167: wrt 706.4,A,B
168: fmt 1,2/,4x,3" DEPTH   TEMP A    TEMP B  "
169: wrt 706.1
170: int(N/3)+1→r2
171: r2*3→r3
172: N-r3+1→r4
173: for I=0 to r2-1;I+r5→r6
174: if r4>=1;r6+1→r6
175: r6+r2+r7→r8
176: if r4>=2;r8+1→r8
177: r8+r2→r9
178: fmt 1,5x,f3.0,4x,f6.3,3x,f6.3,4x,f3.0,4x,f6.3,3x,f6.3,z
179: wrt 706.1,r5,A[r5],B[r5],r7,A[r7],B[r7]
180: fmt 2,4x,f3.0,4x,f6.3,3x,f6.3
181: wrt 706.2,r9,A[r9],B[r9];next I
```

Procedural Step

182: 0+M[4]

Test if Calculation Has Run
Desired Time

183: if M[1]<M[2];gto 190
184: if H[1]<H[2];gto 187
185: if Y[0]<Y[1];gto 187
186: gto 201

Test if Temperature Difference
is to be Calculated

187: M[3]+1+M[3]
188: if M[3]/(r13*20)>=1;gto 190
189: gto 194
190: r13+1+r13

Calculation of Surface and 5-cm
Temperature Difference

191: A[0]-B[0]+U[M[3]/20]
192: A[5]-B[5]+V[M[3]/20]

Calculation of New Time

193: M[3]/60+O[M[3]/20]
194: M[4]+T+M[4]
195: M[1]+T/60+M[1]
196: if M[1]<60;gto 200
197: M[1]-60+M[1]
198: H[1]+1+H[1];if H[1]<24;gto 200
199: H[1]-24+H[1];Y[0]+1+Y[0]
200: gto 99
201: stp

Surface Temperature Difference Plot
of Calculated Data

```
202: deg
203: dsp "SURFACE TEMPERATURE DIFFERENCE";wait 1000;cll 'PLOT'
204: for I=1 to Y[1]*24+H[1];line 1,4;plt I,0;next I
205: pen;line
206: for I=1 to Y[1]*72+3*H[1];if O[I]=0;pen;jmp 2
207: plt O[I],U[I]
208: next I
209: pen
```

5-cm Temperature Difference Plot of
Calculated Data

```
210: dsp "Change Paper,then Continue";stp
211: dsp "5 CM TEMPERATURE DIFFERENCE";wait 1000;cll 'PLOT'
212: for I=1 to Y[1]*24+H[1];line 1,4;plt I,0;next I
213: pen;line
214: for I=1 to Y[1]*72+3*H[1];if O[I]=0;pen;jmp 2
215: plt O[I],V[I]
216: next I
217: pen
218: end
```

Plotting Subroutine

```
219: "PLOT":
220: "POINTS PLOTTED IN MAIN":
221: if flg11;gto +2
222: dim W$[3,50];sfg 11
223: ent "x-min",p4,"x-max",p1,"y-min",p2,"y-max",p3
224: scl p4-(p1-p4)(7/32),p1+(p1-p4)(3/32),p2-(p3-p2)(1/8),p3+(p3-p2)(1/8)
225: ent "x tic interval",p5,"y tic interval",p6
226: csiz 1.5,2,1,0
227: ent "fxd for x-axis",p9
228: fxd p9
229: xax p2,p5,p4,p1,1
230: ent "fxd for y-axis",p10
231: fxd p10
232: yax p4,p6,p2,p3,1
233: prt "IF NO LABEL ENTER DD"
234: ent "bottom label",W$[1]
235: len(W$[1])+p7
236: ent "side label",W$[2]
237: len(W$[2])+p8
238: ent "top label",W$[3]
239: len(W$[3])+p11
240: if W$[1]="DD";gto +2
241: plt (p1-p4)/2+p4,p2-(p3-p2)(1/8),1;cplt -p7/2,0;lbl W$[1]
242: csiz 3,3.5,1,0
243: if W$[3]="DD";gto +2
244: plt (p1-p4)/2+p4,p3+(p3-p2)(1/8),1;cplt -p11/2,0;lbl W$[3]
245: csiz 1.5,2,1,90
246: if W$[2]="DD";gto +2
247: plt p4-(p1-p4)(7/64),(p3-p2)/2+p2,1;cplt -p8/2,0;lbl W$[2]
248: ret
```